nagra.

# Arbeitsbericht NAB 22-02

## TBO Stadel-2-1: Data Report

## Dossier VI Wireline Logging, Micro-hydraulic Fracturing and Pressure-meter Testing

September 2022

J. Gonus, E. Bailey, J. Desroches &
R. Garrard

National Cooperative
for the Disposal of
Radioactive Waste

Hardstrasse 73
P.O. Box
5430 Wettingen
Switzerland
Tel. +41 56 437 11 11

nagra.ch

nagra.

# Arbeitsbericht NAB 22-02

## TBO Stadel-2-1: Data Report

## Dossier VI Wireline Logging, Micro-hydraulic Fracturing and Pressure-meter Testing

September 2022

J. Gonus[1], E. Bailey[1], J. Desroches[1] & R. Garrard[2]

[1] Ad Terra Energy
[2] Nagra

**Keywords:**
STA2-1, Nördlich Lägern, TBO, deep drilling campaign, wireline logging, petrophysical logging, in-situ testing, micro-hydraulic fracturing, pressure-meter testing

**National Cooperative for the Disposal of Radioactive Waste**

Hardstrasse 73
P.O. Box
5430 Wettingen
Switzerland
Tel. +41 56 437 11 11

nagra.ch

Nagra Arbeitsberichte ("Working Reports") present the results of work in progress that have not necessarily been subject to a comprehensive review. They are intended to provide rapid dissemination of current information.

This NAB aims at reporting drilling results at an early stage. Additional borehole-specific data will be published elsewhere.

In the event of inconsistencies between dossiers of this NAB, the dossier addressing the specific topic takes priority. In the event of discrepancies between Nagra reports, the chronologically later report is generally considered to be correct. Data sets and interpretations laid out in this NAB may be revised in subsequent reports. The reasoning leading to these revisions will be detailed there.

This report was finalised in June 2023.

This Dossier was prepared by a project team consisting of:
J. Gonus (petrophysics QC, theoretical concepts and log analysis)
E. Bailey (introductory chapters, BHI QC and project management)
J. Desroches (MHF QC and theoretical concepts)
R. Garrard (coordination and QC review)

Editorial work: P. Blaser and M. Unger

Petrophysical log graphic files were created using Geolog Emerson E&P Software - Emerson Paradigm and Terrastation.

The Dossier has greatly benefitted from reviews by external and internal experts. Their input and work are very much appreciated.

# Table of Contents

## List of Tables

# List of Figures

# List of Appendices



*Note: The Appendices A – F are only included in the digital version of this report and can be found under the paper clip symbol.*

# 1 Introduction

## 1.1 Context

To provide input for site selection and the safety case for deep geological repositories for radioactive waste, Nagra has drilled a series of deep boreholes ("Tiefbohrungen", TBO) in Northern Switzerland. The aim of the drilling campaign is to characterise the deep underground of the three remaining siting regions located at the edge of the Northern Alpine Molasse Basin (Fig. 1-1).

In this report, we present the results from the Stadel-2-1 borehole.

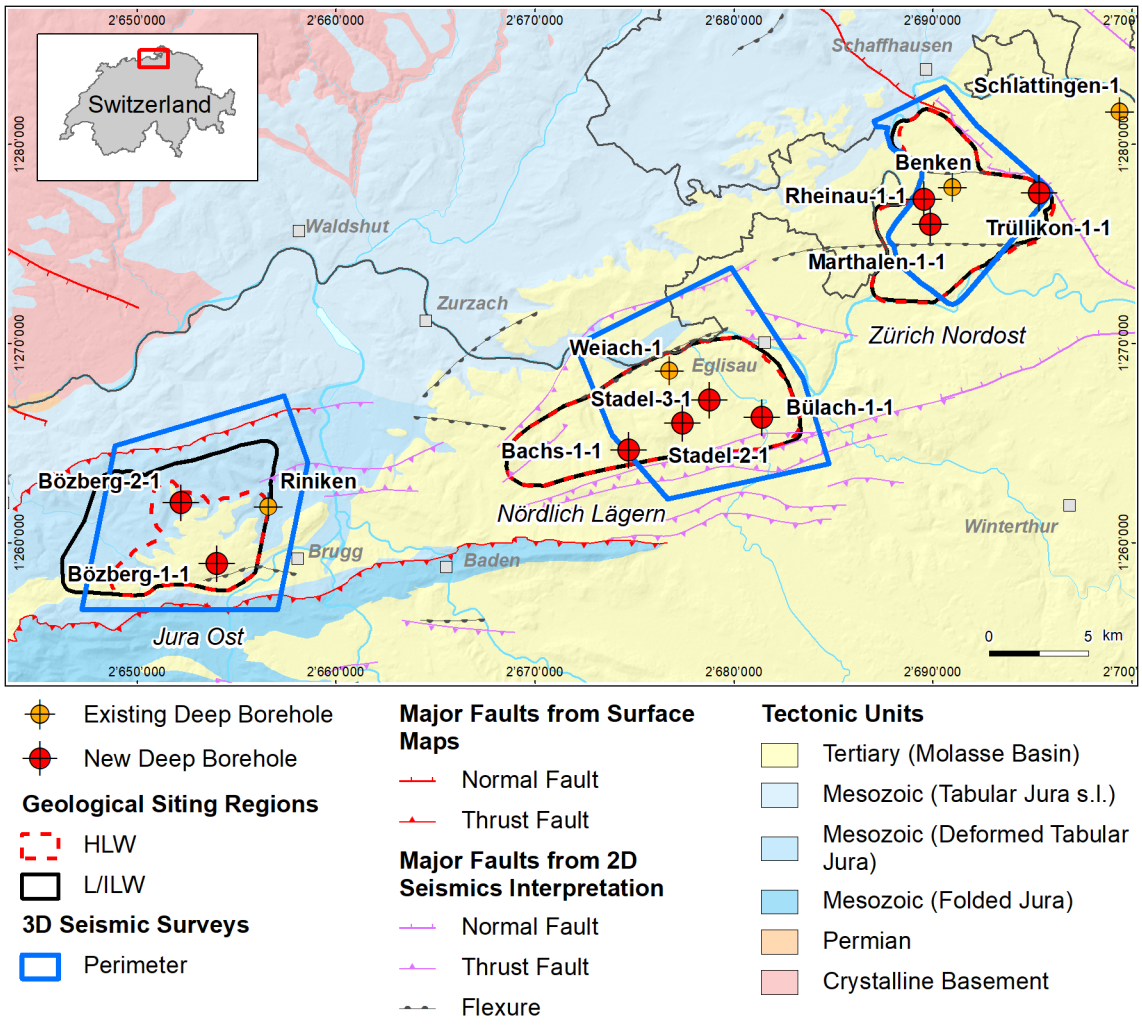


Fig. 1-1: Tectonic overview map with the three siting regions under investigation

## 1.2 Location and specifications of the borehole

The Stadel-2-1 (STA2-1) exploratory borehole is the seventh borehole drilled within the framework of the TBO project. The drill site is located in the central part of the Nördlich Lägern siting region (Fig. 1-2). The vertical borehole reached a final depth of 1'288.12 m (MD)[1]. The borehole specifications are provided in Tab. 1-1.

Tab. 1-1: General information about the STA2-1 borehole

| | |
|---|---|
| **Siting region** | Nördlich Lägern |
| **Municipality** | Stadel (Canton Zürich / ZH), Switzerland |
| **Drill site** | Stadel-2 (STA2) |
| **Borehole** | Stadel-2-1 (STA2-1) |
| **Coordinates** | LV95: 2'677'447.617 / 1'265'987.019 |
| **Elevation** | Ground level = top of rig cellar: 417.977 m above sea level (asl) |
| **Borehole depth** | 1'288.12 m measured depth (MD) below ground level (bgl) |
| **Drilling period** | 25th January – 8th July 2021 (spud date to end of rig release) |
| **Drilling company** | Daldrup & Söhne AG |
| **Drilling rig** | Wirth B 152t |
| **Drilling fluid** | Water-based mud with various amounts of different components such as[2]:<br>0 – 670 m: Bentonite & polymers<br>670 – 1'051 m: Potassium silicate & polymers<br>1'051 – 1'117 m: Water & polymers<br>1'117 – 1'288.12 m: Sodium chloride brine & polymers |

The lithostratigraphic profile and the casing scheme are shown in Fig. 1-3. The comparison of the core versus log depth[3] of the main lithostratigraphic boundaries in the STA2-1 borehole is shown in Tab. 1-2.

[1] Measured depth (MD) refers to the position along the borehole trajectory, starting at ground level, which for this borehole is the top of the rig cellar. For a perfectly vertical borehole, MD below ground level (bgl) and true vertical depth (TVD) are the same. In all Dossiers depth refers to MD unless stated otherwise.

[2] For detailed information see Dossier I.

[3] Core depth refers to the depth marked on the drill cores. Log depth results from the depth observed during geophysical wireline logging. Note that the petrophysical logs have not been shifted to core depth, hence log depth differs from core depth.

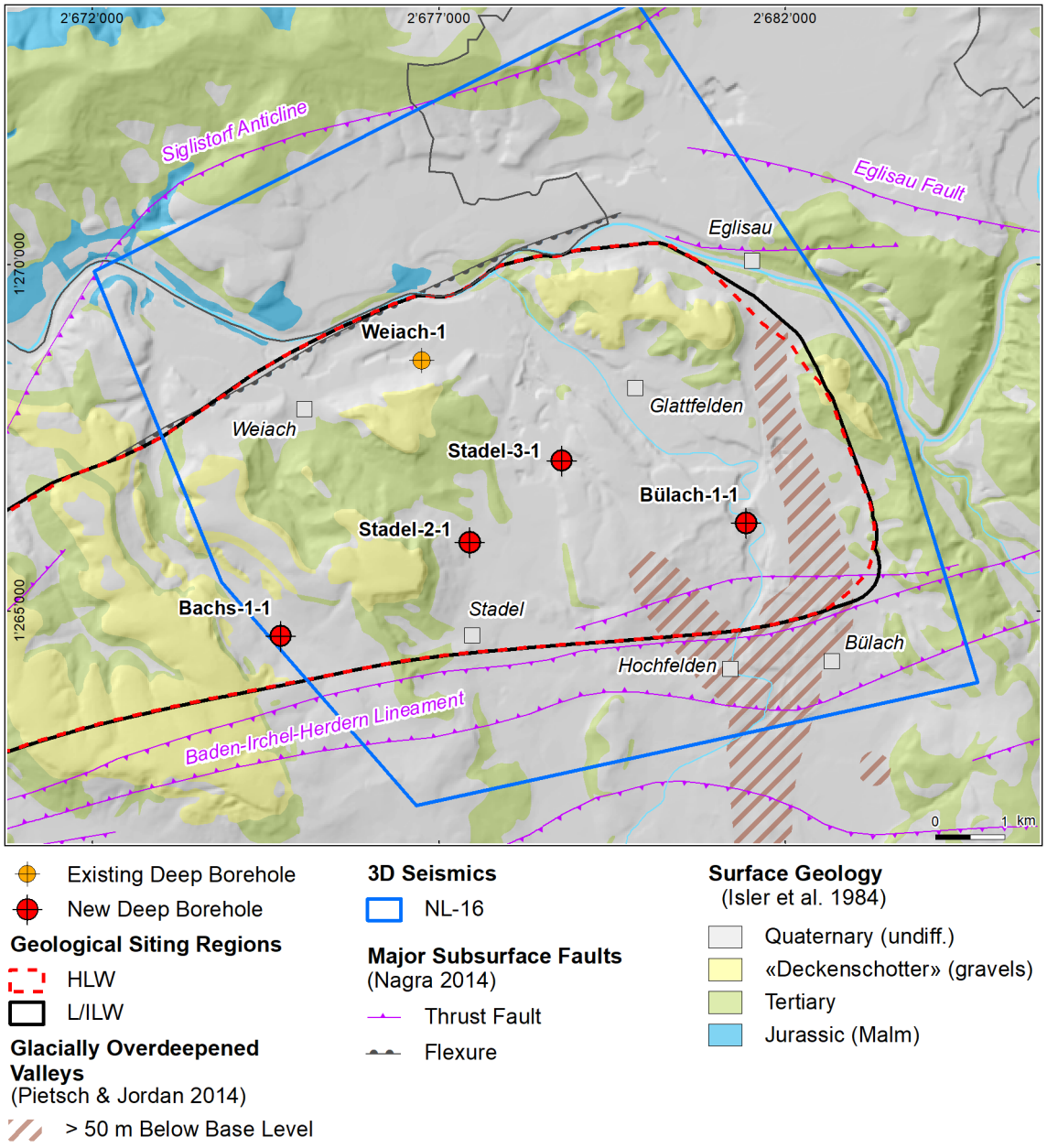


Fig. 1-2: Overview map of the investigation area in the Nördlich Lägern siting region with the location of the STA2-1 borehole in relation to the boreholes Weiach-1, BUL1-1, STA3-1 and BAC1-1

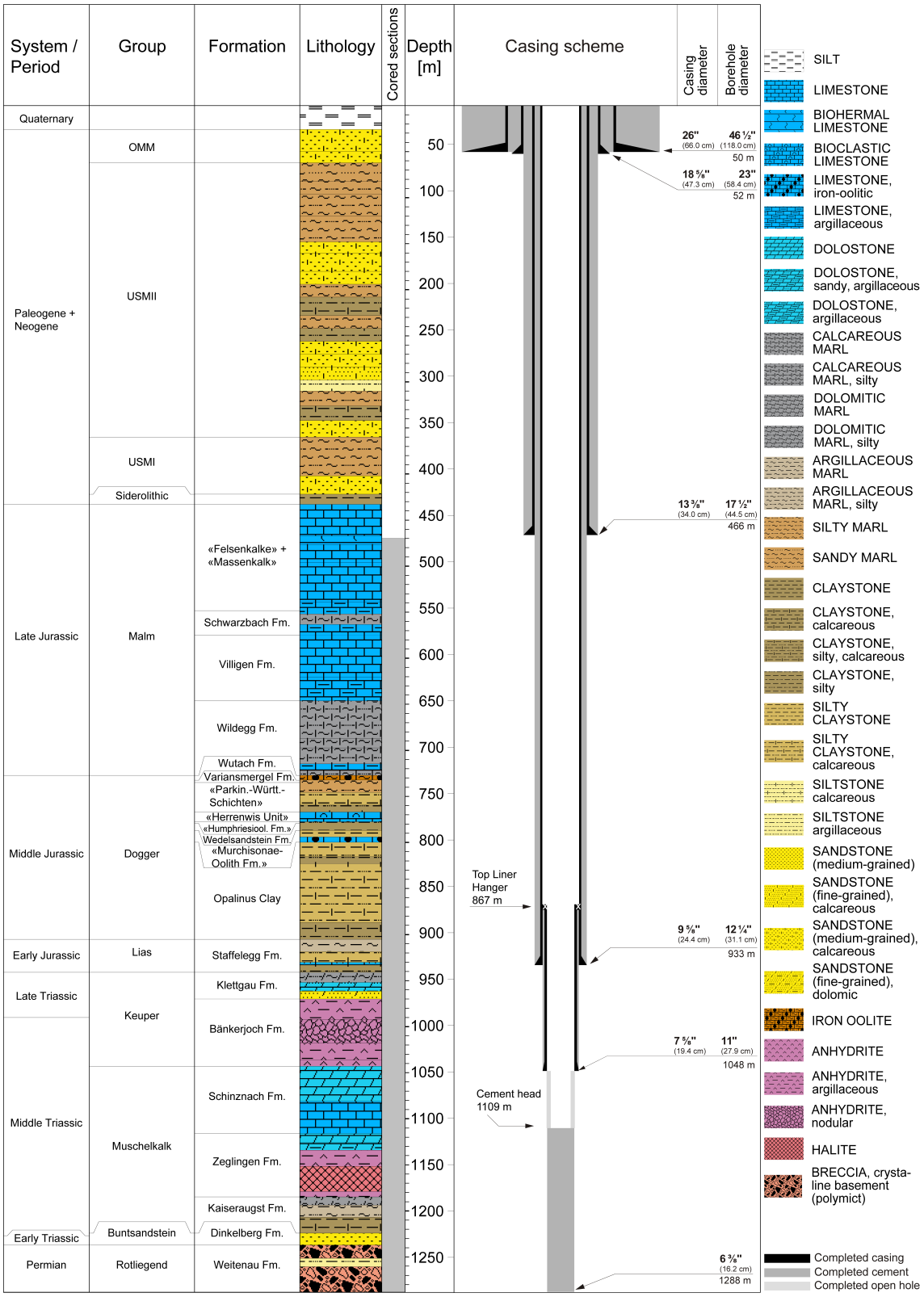


Fig. 1-3: Lithostratigraphic profile and casing scheme for the STA2-1 borehole[4]

[4] For detailed information see Dossier I and III.

Tab. 1-2: Core and log depth for the main lithostratigraphic boundaries in the STA2-1 borehole[5]

| System / Period | Group | Formation | | Core depth in m (MD) | Log depth in m (MD) | |
|---|---|---|---|---|---|---|
| Quaternary | | | | **26.0** | | — |
| Paleogene + Neogene | OMM | | | 62.0 | | — |
| | USM | | | 422.0 | | — |
| | Siderolithic | | | **433.0** | | — |
| Jurassic | Malm | «Felsenkalke» + «Massenkalk» | | 548.35 | 548.62 | — |
| | | Schwarzbach Formation | | 575.08 | 575.45 | — |
| | | Villigen Formation | | 646.23 | 646.63 | — |
| | | Wildegg Formation | | 727.18 | 728.20 | — |
| | Dogger | Wutach Formation | | 732.16 | 733.25 | — |
| | | Variansmergel Formation | | 734.92 | 735.95 | — |
| | | «Parkinsoni-Württembergica-Schichten» | | 767.02 | 768.05 | — |
| | | «Herrenwis Unit» | | 777.54 | 778.47 | — |
| | | «Humphriesioolith Formation» | | 779.34 | 780.27 | — |
| | | Wedelsandstein Formation | | 786.85 | 787.79 | — |
| | | «Murchisonae-Oolith Formation» | | 799.67 | 800.67 | — |
| | | Opalinus Clay | | 905.20 | 906.87 | — |
| | Lias | Staffelegg Formation | | **940.89** | **941.42** | — |
| Triassic | Keuper | Klettgau Formation | | 969.87 | 970.52 | — |
| | | Bänkerjoch Formation | | 1043.07 | 1043.62 | — |
| | Muschelkalk | Schinznach Formation | | 1116.01 | 1116.69 | — |
| | | Zeglingen Formation | | 1184.72 | 1185.42 | — |
| | | Kaiseraugst Formation | | 1224.20 | 1225.07 | — |
| | Buntsandstein | Dinkelberg Formation | | **1237.01** | **1237.94** | — |
| Permian | Rotliegend | Weitenau Formation | final depth | 1288.12 | 1288.87 | |

[5] For details regarding lithostratigraphic boundaries see Dossier III and IV; for details about depth shifts (core goniometry) see Dossier V.

## 1.3 Documentation structure for the STA2-1 borehole

NAB 22-02 documents the majority of the investigations carried out in the STA2-1 borehole, including laboratory investigations on core material. The NAB comprises a series of stand-alone dossiers addressing individual topics and a final dossier with a summary composite plot (Tab. 1-3).

This documentation aims at early publication of the data collected in the STA2-1 borehole. It includes most of the data available approximately one year after completion of the borehole. Some analyses are still ongoing (e.g. diffusion experiments, analysis of veins, hydrochemical interpretation of water samples) and results will be published in separate reports.

The current borehole report will provide an important basis for the integration of datasets from different boreholes. The integration and interpretation of the results in the wider geological context will be documented later in separate geoscientific reports.

Tab. 1-3: List of dossiers included in NAB 22-02

Black indicates the dossier at hand.

| Dossier | Title | Authors |
|---|---|---|
| I | TBO Stadel-2-1: Drilling | P. Hinterholzer-Reisegger |
| II | TBO Stadel-2-1: Core Photography | D. Kaehr & M. Gysi |
| III | TBO Stadel-2-1: Lithostratigraphy | P. Jordan, P. Schürch, H. Naef, M. Schwarz, R. Felber, T. Ibele & H.P. Weber |
| IV | TBO Stadel-2-1: Microfacies, Bio- and Chemostratigraphic Analyses | S. Wohlwend, H.R. Bläsi, S. Feist-Burkhardt, B. Hostettler, U. Menkveld-Gfeller, V. Dietze & G. Deplazes |
| V | TBO Stadel-2-1: Structural Geology | A. Ebert, S. Cioldi, E. Hägerstedt & H.P. Weber |
| VI | TBO Stadel-2-1: Wireline Logging, Micro-hydraulic Fracturing and Pressure-meter Testing | J. Gonus, E. Bailey, J. Desroches & R. Garrard |
| VII | TBO Stadel-2-1: Hydraulic Packer Testing | R. Schwarz, R. Beauheim, S.M.L. Hardie & A. Pechstein |
| VIII | TBO Stadel-2-1: Rock Properties, Porewater Characterisation and Natural Tracer Profiles | C. Zwahlen, L. Aschwanden, E. Gaucher, T. Gimmi, A. Jenni, M. Kiczka, U. Mäder, M. Mazurek, D. Roos, D. Rufer, H.N. Waber, P. Wersin & D. Traber |
| IX | TBO Stadel-2-1: Rock-mechanical and Geomechanical Laboratory Testing | E. Crisci, L. Laloui & S. Giger |
| X | TBO Stadel-2-1: Petrophysical Log Analysis | S. Marnat & J.K. Becker |
| | TBO Stadel-2-1: Summary Plot | Nagra |

## 1.4 Scope and objectives of this dossier

The dossier at hand describes the acquisition, quality control and results of the Petrophysical Logging (PL), Micro-hydraulic Fracturing (MHF) and Pressure-meter Testing (PMT) wireline logging measurements performed in the STA2-1 borehole.

Petrophysical log measurements were acquired in open borehole conditions (no casing) with wire-line conveyed logging tools to determine continuous profiles across the borehole of physical and chemical properties of the formation, including its mineralogy, clay types, porosity, fluid content, and acoustic properties. Petrophysical logs were further acquired to obtain high-resolution circumferential images of the borehole wall, as well as to measure borehole physical parameters such as its geometry, mud resistivity and mud temperature. In addition to the open hole logs, temperature logs were acquired post-completion to measure the undisturbed mud temperature.

A series of in situ stress measurements were performed using the micro-hydraulic fracturing technique to estimate the orientation and magnitude of the earth stress at different depths. The objectives of the MHF testing programme were to provide estimates of the in-situ stress state in the Opalinus Clay potential rock host and adjacent rock formations and provide calibration points for mechanical earth models (MEM) of the rock mass (both 1D and 3D).

Pressure-meter testing was performed at the same time as MHF testing using the same module that was used to perform sleeve fracturing and sleeve reopening during MHF operations. The objective of the PMT programmes in the Stadel 3-1 and Stadel 2-1 (STA2-1) boreholes were to obtain an interpretable pressure record in the Opalinus Clay from which the in-situ shear modulus can be estimated for comparison with the dilatometer tests. Due to a malfunction of the University of Alberta's (UoA) dilatometer tool, no data could be acquired in STA2-1 and therefore shall not be discussed further in this report.

All PL, MHF and PMT testing were performed by the wireline logging company Schlumberger (SLB). Ad Terra Energy (formerly Geneva Petroleum Consultants International) were responsible for planning wireline operations, technical supervision at the worksite, quality assurance and control (QA-QC) of data, database management and general wireline logging support.

This dossier is organised as follows:

- Chapter 2: The sequence of events for PL, MHF and PMT testing operations, and associated log / data coverage is provided.
- Chapter 3: The QA-QC procedure used to assess the quality of the petrophysical logs is detailed. A continuous profile of each log across the entire measured depth of the borehole is quality-controlled, corrected and spliced together to generate a quality-controlled composite log. The results of the composite log are discussed. The composite log will then be used as the final log data for input into further data analysis processes such as formation evaluation (e.g. Stochastic Petrophysical Log Analysis described in Dossier X), calibration with seismic data and integration with sedimentology and structural geology data (from cores, cuttings, adjacent boreholes and regional geology).
- Chapter 4: Although Borehole Imagery (BHI) logs were acquired as a part of the petro-physical logging, the objectives of BHI are related to both Structural Geology (analysis of image features described in Dossier V) and MHF / PMT (firstly the selection of stations for stress measurements, then the analysis of fractures induced by tests). Thus, the QC, pro-cessing and interpretation processes of BHI are described in a chapter separate from the QA-QC procedures of the other petrophysical logs in Chapter 3.

- Chapter 5: MHF test procedures and preliminary results are presented.
- Chapter 6: PMT test procedures and preliminary results are presented.
- Finally, this report includes a set of appendices, where spliced PL, pre- and post-MHF / PMT borehole images and MHF / PMT data can be found.

# 2 Wireline logging and testing operations

The STA2-1 borehole was planned in 4 drilling sections. After installation of the 26" and 18⅝" outer diameter (OD) conductor casings, Section I was drilled with the 17½" drill bit and one petrophysical logging run was undertaken before installing the 13⅜" OD casing. Sections II through IV were cored with the 6⅜" core bit in two parts, to ensure optimum borehole conditions for fluid logging, hydraulic testing and petrophysical logging. Once section TD was reached, petrophysical logs were acquired continuously over the section, before reaming (opening up) to 8½" for dilatometer, MHF and PMT testing. After logging / testing operations were completed in Sections II and III, the borehole was reamed to 12¼" and 11" for installation of the 9⅝" casing and 7⅝" liner, respectively. Once open borehole logging / testing operations were completed, the borehole was backfilled with cement up from 1'288.12 to 1'109.00 m MD. One post-completion, petrophysical log was acquired to measure the undisturbed mud temperature. Detailed descriptions of the borehole design and mud conditions at the time of logging and testing are included in the excel Composite Report (Appendix A), under the worksheets entitled 'Borehole design' and 'Hole & mud system'. Additional details about borehole configuration, casing and cementing scheme and mud parameters can be found in Dossier I.

Wireline logging and testing operations were divided into the following groups of activities:

- Petrophysical Logging (PL)
- Micro-hydraulic Fracturing (MHF)
- Pressure-meter Testing (PMT)
- *Technical Logging (TL)*
- *Vertical Seismic Profiling (VSP)*

Petrophysical logs are continuous measurements (normally recorded every half foot or approximately 15 cm) of mineralogy and physical properties of formation rocks, their contained fluids, and the borehole environment between the wireline conveyed logging tool sensors and the borehole wall. Petrophysical logs were acquired with conventional and advanced wireline-conveyed logging tools. Conventional tools measured Depth (measured depth [MD], or log depth, that is the depth reference for all wireline measurements), Total Gamma Ray (naturally occurring gamma radiation), Spontaneous Potential (electric potential difference between the formation and an electrode at surface), Temperature, Caliper (measurement of the borehole diameter), Inclinometer (measurement of the borehole trajectory), as well as the standard "quad combo" tools: Resistivity (electrical resistivity at different depths of investigation in the formation), Sonic (compressional and shear wave slowness), Density (measurement of the bulk density and the photoelectric factor), and Neutron (measurement of the neutron hydrogen index, a proxy of porosity, as well as the sigma capture cross-section). Advanced tools measured the Spectral Gamma Ray (potassium, thorium and uranium contributions to the total naturally occurring gamma radiation), Elemental Spectroscopy, and Microresistivity and Ultrasonic borehole images. These logging tools and their main measurements are described in detail in the subsequent Chapter 3 – Petrophysical Logging and Chapter 4 – Borehole Imagery.

MHF involves using wireline-conveyed testing equipment to initiate and analyse the characteristics of micro-hydraulic fractures through several opening / closure cycles, to estimate the current stress state in the rock formation at the 1 m scale. Tests were conducted using the SLB Modular Formation Dynamics Tester (MDT), which uses packer modules, surface-controlled downhole valves, downhole pressure gauges and a downhole pump to initiate and propagate fractures at predefined discrete depths. MHF tests are described in Chapter 5 – Micro-hydraulic Fracturing.

PMT was conducted using the single packer module from the MDT tool that is used to perform sleeve fracturing and reopening operations during MHF testing. PMT previously undertaken in the BOZ1-1 and BOZ2-1 boreholes explored different tool string combinations and protocols to find the best possible hardware / methodology for obtaining an interpretable pressure record in the formation of interest. Based on the results of these tests, PMT was undertaken using a reduced protocol and the Frac12k packer. PMT tests are described in Chapter 6 – Pressure-meter Testing.

As well as PL, MHF and PMT operations, wireline operations also included Technical Logging (TL) and Vertical Seismic Profiling (VSP). TL acquired data on the physical properties of the open borehole (geometry and trajectory) and the permanent casing installation. The borehole geometry was measured using calipers for both assessing the borehole condition (breakouts / washouts present) and determining the volume of cement needed for casing installations. The borehole inclination and azimuth were measured to confirm the borehole verticality and identify its trajectory. To assess the quality of the cement behind the casing, Cement Bond Logs (CBL) and acoustic impedance logs were acquired using a sonic (MSIP) and ultrasonic imaging (USIT) tools. Borehole deviation surveys, cement volume calculations and CBL logs are described in Dossier I. VSP acquired high resolution borehole seismic measurements used for correlation with, and enhancement of, surface seismic data. VSP will be addressed in a separate document. TL and VSP are not described further in this report.

A summary of all wireline logging and testing activities carried out in the STA2-1 borehole is given in Tab. 2-1. Fig. 2-1 depicts graphically the log coverage for the PL, MHF and PMT testing campaigns. In total, 6 PL, 3 MHF and 1 PMT testing campaign were undertaken. Open hole PL was conducted in all sections of STA2-1, whilst MHF testing was conducted in Sections II to IV. PMT was focused on the Opalinus Clay host rock and therefore only undertaken in Section II. A more detailed analysis of the log measurement coverage is provided in Chapter 3.

Details of the logging runs, logging dates, wireline logging company, logging interval, logging suite and principal measurements acquired for PL, MHF and PMT operations are provided in Tab. 2-2. Mnemonics for each tool in the logging suite listed in this table are given in Tab. 2-3.

Tab. 2-1: Logging and testing activities during drilling of the STA2-1 borehole

| **Drilling phase / section** | **Permanent casing size at time of logging**<br><br>**Casing / liner shoe depth** | **Open hole interval and bit size** | **Start date** | **End date** | **Coring** | **Technical logging** | **Petrophysical logging** | **Micro-hydraulic fracturing** | **Pressure-meter testing** | **Vertical seismic profiling** |
|---|---|---|---|---|---|---|---|---|---|---|
| I | 18⅝"<br>0 to 52.00 m | 52.00 to 467.00 m in 17½" | 22.01.2021 | 05.02.2021 | | | × | | | |
| II | 13⅜"<br>0 to 466.00 m | 466.00 to 470.00 in 12¼"<br>470.00 to 670.00 m 6⅜" | 05.02.2021 | 13.05.2021 | × | × | | | | |
| | | 466.00 to 470.00 in 12¼"<br>470.00 to 936.00 m 6⅜" | | | × | | × | | | |
| | | 466.00 to 470.00 in 12¼"<br>470.00 to 933.50 m 8½"<br>933.50 to 936.00 m 6⅜" | | | | | × | × | × | |
| | | 466.00 to 936.00 m in 12¼" | | | | × | | | | |
| III | 9⅝"<br>0 to 933.00 m | 933.00 to 938.00 m in 8½"<br>938.00 to 1'051.00 m 6⅜" | 13.05.2021 | 11.06.2021 | × | | × | | | |
| | | 933.00 to 1'051.00 m in 8½" | | | | | × | × | | |
| | | 933.00 to 934.00 in 8½"<br>934.00 to 1'051.00 in 9½" | | | | × | | | | |
| | | 933.00 to 934.00 in 8½"<br>934.00 to 1'050.00 in 11½"<br>1'050.00 to 1'051.00 in 9½" | | | | × | | | | |
| IV | 7⅝"<br>867.00 to 1'048.00 m | 1'048.00 to 1'053.00 in 6½"<br>1'053.00 to 1'288.12 in 6⅜" | 11.06.2021 | 08.07.2021 | × | × | × | × | | × |

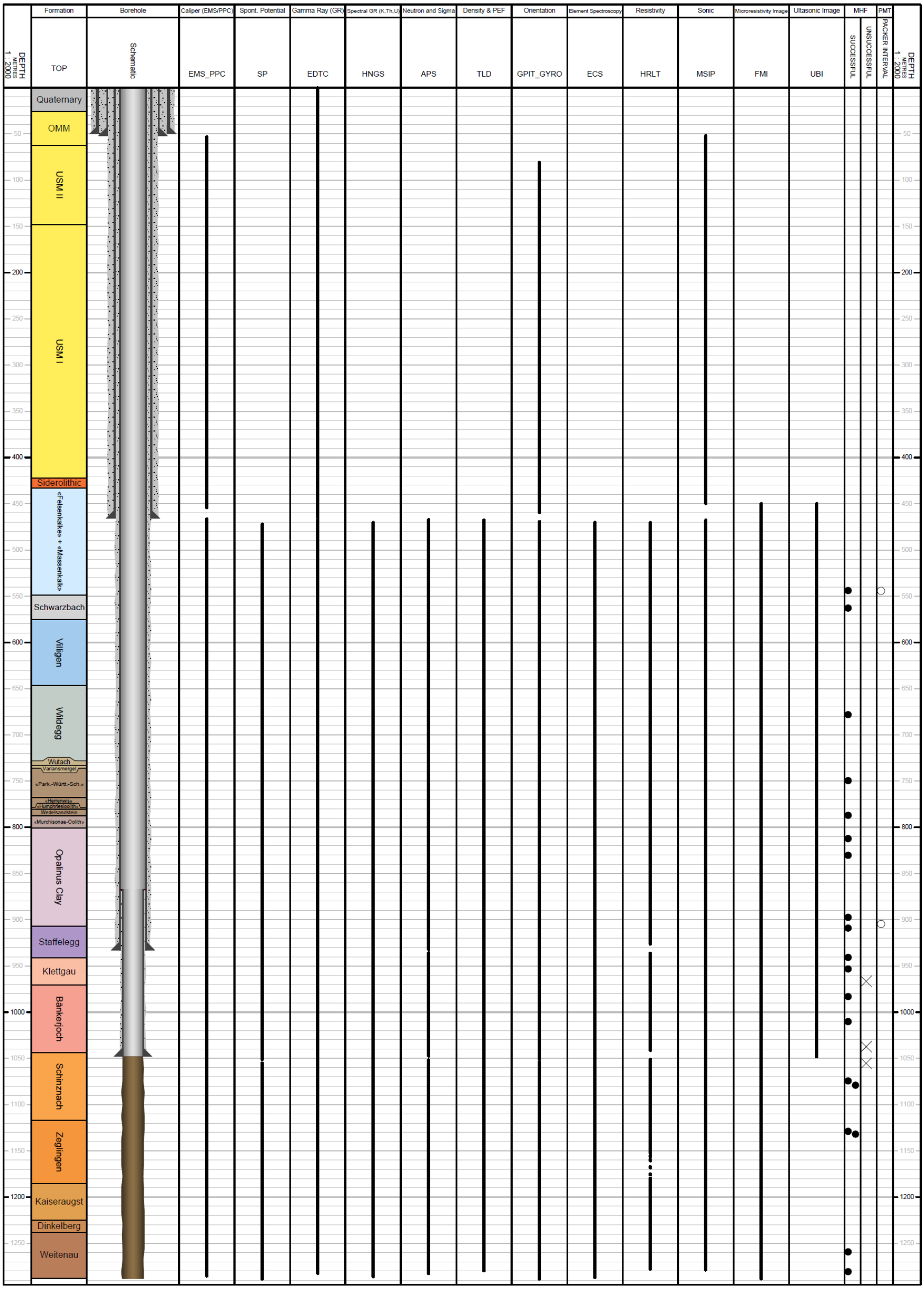


Fig. 2-1: Petrophysical log, MHF and PMT testing coverage at STA2-1 (scale of 1:2'000)

Tab. 2-2: Logging and testing sequence of events (only PL, MHF and PMT)

| **Phase / Section** | **Run** | **Operation** | **Logging date** | **Contractor** | **Logging interval** [m MD] | **Logging suite** (see list of abbreviations) | **Measurements** | | | | | | | | | | | | | | | | **Remarks** |
|---|---|---|---|---|---|---|---|---|---|---|---|---|---|---|---|---|---|---|---|---|---|---|---|
| | | | | | | | **Gamma ray** | **Resistivity** | **Microresistivity** | **Density** | **Sonic** | **Neutron hydrogen index** | **Sigma capture cross-section** | **Photoelectric factor** | **Spontaneous potential** | **Borehole imaging** | **Caliper** | **Spectral gamma ray** | **Elemental spectroscopy** | **Inclinometer** | **Temperature** | **MHF / PMT / Dilatometer** | |
| I | 1.1.1 | PL | 01.02.2021 | SLB | 20.00 to 455.00 | PPC-MSIP-PPC-GPIT-EMS-EDTC-LEH.QT | × | | | | × | | | | | | × | | | × | | | Poor quality sonic due to large hole |
| II | 2.1.1 | PL | 16. – 17.03.2021 | SLB | 450.00 to 929.40 | FMI-EMS-EDTC-LEH.QT | × | | | | | | | | | × | × | | | × | × | | |
| | 2.1.2 | | 17.03.2021 | SLB | 450.00 to 927.70 | PPC-MSIP-PPC-GPIT-EDTC-LEH.QT | × | | | | × | | | | | | × | | | × | | | |
| | 2.1.3 | | 17.03.2021 | SLB | 450.00 to 935.60 | TLD-MCFL-EDTC-LEH.QT | × | | × | × | | | | × | | | | | | | | | |
| | 2.1.4 | | 17. – 18.03.2021 | SLB | 450.00 to 932.20 | APS-EMS-EDTC-LEH.QT | × | | | | | × | × | | | | × | | | | × | | |
| | 2.1.5 | | 18.03.2021 | SLB | 450.00 to 936.20 | ECS-EDTC-LEH.QT | × | | | | | | | | | | | | × | | | | |
| | 2.1.6 | | 18.03.2021 | SLB | 450.00 to 933.80 | HNGS-EDTC-LEH.QT | × | | | | | | | | | | | × | | | | | |
| | 2.1.7 | | 18.03.2021 | SLB | 450.00 to 934.00 | SP-EMS-HRLT-EDTC-LEH.QT | × | × | | | | | | | × | | × | | | | × | | |
| | 2.2.1 | PL | 11. – 12.04.2021 | SLB | 450.00 to 934.00 | UBI-GPIT-EDTC-LEH.QT | × | | | | | | | | | × | | | | × | | | Acquired before GTPT / hydrotests to measure possible convergence of the borehole |
| | 2.3.1 | PL | 25. – 26.04.2021 | SLB | 450.00 to 932.00 | UBI-GPIT-EDTC-LEH.QT | × | | | | | | | | | × | | | | × | | | Acquired after GTPT / hydrotests to measure possible convergence of the borehole |
| | 2.4.1 | PL | 30.04.2021 | SLB | 450.00 to 934.00 | EMS-EDTC-LEH.QT | × | | | | | | | | | | × | | | | × | | |

Tab. 2-2: continued

| Phase / Section | Run | Operation | Logging date | Contractor | Logging interval [m MD] | Logging suite (see list of abbreviations) | Measurements | | | | | | | | | | | | | | | | Remarks |
|---|---|---|---|---|---|---|---|---|---|---|---|---|---|---|---|---|---|---|---|---|---|---|---|
| | | | | | | | Gamma ray | Resistivity | Microresistivity | Density | Sonic | Neutron hydrogen index | Sigma capture cross-section | Photoelectric factor | Spontaneous potential | Borehole imaging | Caliper | Spectral gamma ray | Elemental spectroscopy | Inclinometer | Temperature | MHF / PMT / Dilatometer | |
| II | 2.4.2 | Dilatometer | 30.04. – 01.05.2021 | SLB / UOA | n/a | DILA--LEH.QT | | | | | | | | | | | | | | | | × | Unsuccessful run - no data acquired due to failure of the dilatometer tool |
| | 2.4.3 | MHF | 01. – 04.05.2021 | SLB | 9 stations | MRPA(dual)-MRSF(single)-MRSC(exit)-MRSC(forced closure)-MRPO(XP)-5xMRSC(water)-MRSC(exit)-MRPC-EDTC-LEH.QT | | | | | | | | | | | | | | | | × | 9 successful MHF tests out of 9; 1 PMT test + 1 calibration |
| | 2.4.4 | PL | 04.05.2021 | SLB | 450.00 to 932.70 | FMI-EDTC-LEH.QT | × | | | | | | | | | × | × | | | × | | | Post-MHF |
| III | 3.1.1 | PL | 27.05.2021 | SLB | 890.00 to 1'039.83 | FMI-EMS-EDTC-LEH.QT | × | | | | | | | | | × | × | | | × | × | | |
| | 3.1.2 | | 27.05.2021 | SLB | 900.00 to 1'042.50 | PPC-MSIP-PPC-GPIT-EDTC-LEH.QT | × | | | | × | | | | | | × | | | × | | | |
| | 3.1.3 | | 28.05.2021 | SLB | 920.00 to 1'050.00 | TLD-MCFL-EDTC-LEH.QT | × | | × | × | | | | × | | | | | | | | | |
| | 3.1.4 | | 28.05.2021 | SLB | 920.00 to 1'048.00 | APS-EMS-EDTC-LEH.QT | × | | | | | × | × | | | | × | | | | × | | |
| | 3.1.5 | | 28.05.2021 | SLB | 920.00 to 1'049.72 | ECS-EDTC-LEH.QT | × | | | | | | | | | | | | × | | | | |
| | 3.1.6 | | 28.05.2021 | SLB | 920.00 to 1'048.71 | HNGS-EDTC-LEH.QT | × | | | | | | | | | | | × | | | | | |
| | 3.1.7 | | 28.05.2021 | SLB | 920.00 to 1'041.45 | SP-EMS-HRLT-EDTC-LEH.QT | × | × | | | | | | | × | | × | | | | × | | |
| | 3.2.1 | PL | 30. – 31.05.2021 | SLB | 916.00 to 1'050.40 | EMS-EDTC-LEH.QT | × | | | | | | | | | | × | | | | × | | |
| | 3.2.2 | | 31.05.2021 | SLB | 920.00 to 1'048.20 | UBI-GPIT-EDTC-LEH.QT | × | | | | | | | | | × | | | | × | | | |

Tab. 2-2: continued

| Phase / Section | Run | Operation | Logging date | Contractor | Logging interval [m MD] | Logging suite (see list of abbreviations) | Measurements | | | | | | | | | | | | | | | | Remarks |
|---|---|---|---|---|---|---|---|---|---|---|---|---|---|---|---|---|---|---|---|---|---|---|---|
| | | | | | | | Gamma ray | Resistivity | Microresistivity | Density | Sonic | Neutron hydrogen index | Sigma capture cross-section | Photoelectric factor | Spontaneous potential | Borehole imaging | Caliper | Spectral gamma ray | Elemental spectroscopy | Inclinometer | Temperature | MHF / PMT / Dilatometer | |
| III | 3.2.3 | MHF | 31.05. – 02.06.2021 | SLB | 6 stations | MRPA(dual)-MRSF(single)-MRSC(exit)-MRSC(forced closure)-MRPO(XP)-4xMRSC(water)-MRSC(exit)-MRPC-EDTC-LEH.QT | | | | | | | | | | | | | | | | × | 5 successful MHF tests out of 6; Dual packers could not seal and hold pressure in the interval and were therefore replaced between runs 3.2.3 and 3.2.4. |
| | 3.2.4 | | 02. – 03.06.2021 | SLB | | | | | | | | | | | | | | | | | | × | |
| | 3.2.5 | PP | 05.06.2021 | SLB | 920.00 to 1'050.65 | FMI-EDTC-LEH.QT | × | | | | | | | | | × | | | | × | | | Post-MHF |
| IV | 4.1.1 | PL | 28. – 29.06.2021 | SLB | 1'052.00 to 1'288.40 | FMI-EMS-EDTC-LEH.QT | × | | | | | | | | | × | × | | | × | × | | |
| | 4.1.2 | | 29.06.2021 | SLB | 1'035.00 to 1'286.00 | HNGS-EDTC-LEH.QT | × | | | | | | | | | | | × | | | | | VSP took place between runs 4.1.2 and 4.1.4 |
| | 4.1.4 | | 29. – 30.06.2021 | SLB | n/a | UBI-GPIT-EDTC-LEH.QT | × | | | | | | | | | × | | | | × | | | The tool could not pass below 1'081.70 m MD, therefore run was abandoned |
| | 4.1.5 | | 30.06.2021 | SLB | 1'025.00 to 1'288.74 | SP-EMS-HRLT-EDTC-LEH.QT | × | × | | | | | | | × | | × | | | | × | | |
| | 4.1.6 | | 30.06.2021 | SLB | 1'020.00 to 1'281.00 | PPC-MSIP-PPC-GPIT-EDTC-LEH.QT | × | | | | × | | | | | | × | | | × | | | |
| | 4.1.7 | | 30.06. – 01.07.2021 | SLB | 1'035.00 to 1'281.50 | APS-TLD-MCFL-EDTC-LEH.QT | × | | × | × | | × | × | × | | | × | | | | × | | TLD and APS were combined |
| | 4.1.8 | | 01.07 – 03.07.2021 | SLB | 1'033.00 to 1'086.80 | ECS-EDTC-LEH.QT | × | | | | | | | | | | | | × | | | | |

Tab. 2-2: continued

| Phase / Section | Run | Operation | Logging date | Contractor | Logging interval [m MD] | Logging suite (see list of abbreviations) | Measurements | | | | | | | | | | | | | | | | Remarks |
|---|---|---|---|---|---|---|---|---|---|---|---|---|---|---|---|---|---|---|---|---|---|---|---|
| | | | | | | | Gamma ray | Resistivity | Microresistivity | Density | Sonic | Neutron hydrogen index | Sigma capture cross-section | Photoelectric factor | Spontaneous potential | Borehole imaging | Caliper | Spectral gamma ray | Elemental spectroscopy | Inclinometer | Temperature | MHF / PMT / Dilatometer | |
| IV | 4.1.9 | MHF | 03.07.2021 | SLB | 2 stations | MRPA(dual)-MRPA(single)-MRSC(exit)-MRSC(forced closure)-MRPO(XP)-4xMRSC(water)-MRSC(exit)-MRPC-EDTC-LEH.QT | | | | | | | | | | | | | | | | × | 2 successful MHF tests out of 2; The MDT tool string got stuck after MHF Station 1-2; the electrically controlled release device (ECRD) was released and the wireline POOH; the tool string was fished out and a wiper trip was performed |
| | 4.2.1 | PP | 03. – 05.07.2021 | SLB | 1'035.00 to 1'161.60 | EMS-EDTC-LEH.QT | × | | | | | | | | | | × | | | | × | | Additional run after fishing the MDT tool and the wiper trip to assess the shape of the borehole |
| | 4.2.2 | MHF | 05.07.2021 | SLB | 5 stations | MRPA(dual)-MRPA(single)-MRSC(exit)-MRSC(forced closure)-MRPO(XP)-4xMRSC(water)-MRSC(exit)-MRPC-EDTC-LEH.QT | | | | | | | | | | | | | | | | × | 4 successful MHF tests out of 5 |
| | 4.2.3 | PP | 05.07.2021 | SLB | 1'052.00 to 1'276.00 | FMI-EMS-EDTC-LEH.QT | × | | | | | | | | | × | × | | | × | × | | Post-MHF |
| | 4.3.1 | PP | 04.07.2022 | SLB | 0 to 1'108.10 | EMS-EDTC-LEH.QT | × | | | | | | | | | | × | | | | × | | Post completion |

Tab. 2-3: Tool mnemonics and measurement details

| **Logging tool** | **Wireline contractor** | **Mnemonic** | **Principal measurement** |
|---|---|---|---|
| APS | SLB | Accelerator porosity sonde | Epithermal and thermal neutrons, sigma capture cross-section of thermal neutrons |
| ECS | SLB | Elemental capture spectroscopy sonde | Measurement of the relative dry weight element concentration (e.g. Si, Ca, Fe, S, Ti, Gd, Cl and H) and mineralogical model |
| EDTC | SLB | Enhanced digital telemetry cartridge | Gamma ray measurement of the total natural radioactivity |
| EMS | SLB | Environmental measurement sonde | 6-arm caliper, temperature and mud resistivity |
| FMI | SLB | Fullbore formation microimager | Microresistivity imaging tool (pad contact) |
| GPIT | SLB | General purpose inclinometry tool | Orientation/inclination of the borehole |
| HNGS | SLB | Hostile natural gamma ray sonde | Spectral gamma ray measurements of natural radioactivity (potassium, thorium, uranium) |
| HRLT | SLB | High resolution laterolog array tool | Laterolog resistivity measurement at different depths of investigation |
| LEH.QT | SLB | Logging equipment head with tension | Head tension |
| MCFL | SLB | Microcylindrically focused log | Measures the invaded zone resistivity (RXO) |
| MRPA | SLB | Packer modules | Packer modules for stress measurements:<br>- Dual (straddle) for MHF tests<br>- Single for sleeve fracturing, sleeve reopening and PMT tests |
| MRPO | SLB | Pump out module | Downhole pump for MHF / PMT tests |
| MRSC | SLB | Sample chamber | Typically used to carry fluid for MHF / PMT tests, usually filled with water; can also be configured as an exit port |
| MSIP | SLB | Modular sonic imaging platform (sonic scanner) | Compressional, shear and Stoneley wave slowness measurements (monopole and dipole sources); cement bond log |
| PPC | SLB | Power positioning calipers | 4-arm caliper that gives dual axis borehole measurements |
| SP | SLB | Spontaneous potential | Measurement of electrical potential difference between the borehole and the surface |
| TLD | SLB | Three-detector lithology density | Bulk density and photoelectric absorption factor measurement |
| UBI | SLB | Ultrasonic borehole imager | High-resolution acoustic (ultrasonic) images of the borehole |

# 3 Petrophysical Logging (PL)

## 3.1 Petrophysical logging tools and measurements

Below the main petrophysical measurements acquired, and the downhole logging tools deployed are summarised. A detailed description of how the different tools measure the respective parameters and the underlying physics behind these measurements is not the focus of this report. Borehole imaging tools are described in Chapter 4.

- **Borehole deviation / orientation** (GPIT – General Purpose Inclinometry Tool). The GPIT outputs inclinometer measurements. Tool orientation is defined by three parameters: tool deviation, tool azimuth and relative bearing. Borehole trajectory is calculated from the inclinometer measurements. Inclinometer measurements serve to reference the oriented logs (e.g. borehole imagery and sonic dipole logs).
- **Caliper log** (EMS/PPC – Environmental Measurement Sonde/Powered Positioning Caliper). The caliper log uses several coupled pairs of mechanical arms (2 pairs with PPC, 3 pairs with EMS) to continuously measure the borehole shape in different orientations.
- **Density** (TLD – Three-detector Lithology Density). TLD is an induced radiation tool that measures the bulk density of the formation and the photoelectric factor (PEF). It uses a radioactive source to emit gamma photons into the formation. The gamma rays undergo Compton scattering by interacting with the atomic electrons in the formation. Compton scattering reduces the energy of the gamma rays in a stepwise manner and scatters the gamma rays in all directions. When the energy of the gamma rays is less than 0.5 MeV, they can undergo photoelectric absorption by interacting with the electrons. The flux of gamma rays that reach each of the detectors of the TLD is therefore attenuated by the formation, and the amount of attenuation is dependent upon the density of electrons in the formation, which is related to its bulk density. The bulk density of a rock is the sum of the minerals (solids) and fluids volumes (porosity) times their densities. Hence, the formation density tool is key for the determination of porosity, the detection of low-density fluids (gasses) in the pores and mineralogical identification. In addition, the TLD provides the **photoelectric absorption index** (photoelectric factor – PEF), which represents the probability that a gamma photon will be photoelectrically absorbed per electron of the atoms that compose the material. The PEF characterises the mineralogy. The TLD tool is housed in the High-Resolution Mechanical Sonde that also includes the Micro-Cylindrically Focused Log (MCFL) sonde, that measures the **microresistivity** or alternatively, the resistivity very close to the borehole wall (RXOZ). The bulk density was integrated over depth, to provide the overburden pressure or vertical stress (Sv).
- **Element Spectroscopy** (ECS – Elemental Capture Spectroscopy). The ECS is also an induced radiation tool with a radioactive neutron source. The ECS measures the concentration of a series of elements in the formation (Si, Ca, Fe, S, Ti, Gd, Cl, H) by analysing the gamma ray spectrum of back scattered gamma rays. Special processing techniques allow under certain circumstances the measurement of supplementary elements such as Al, Mg, K and Na. The element spectroscopy measurements are provided in dry weight concentrations. SLB uses an algorithm in the field to derive a model of dry weight fractions of preset minerals from the dry weight element concentrations: clay, clastics (quartz – feldspar – mica, QFM), carbonates, anhydrite / gypsum, salt / evaporite, pyrite, siderite and coal. Advanced models can discriminate limestone and dolomite from carbonates, as well to provide a more quantitative clay measurement. It is important to note that mineralogy model processing is qualitative and should be viewed as an indicator of lithology and not used in any quantitative analysis. Quantitative analysis of the ECS dry weight elements needs to be calibrated against core data.

Dossier X details stochastic processing and interpretation of the ECS dry weight proportions, combined with conventional petrophysical log response, to generate a quantified lithology determination.

- **Gamma Ray** (GR, from the EDTC – Enhanced Digital Telemetry Cartridge). This log measures the total naturally occurring gamma ray radioactivity in the formation rocks (potassium, thorium and uranium are the most common radioactive elements in Earth's crust), which can be used to determine the volume of clay minerals (that contains those elements). The GR log is not valid for clay determination if other minerals contain those elements in significant amounts (e.g. potassic feldspars, organic matter, phosphates). The GR is run with all logging runs because it is used for depth correlation between runs, thanks to its excellent vertical resolution and character. Note this is not to be confused with the Spectral Gamma Ray which is a different tool detailed further below.
- **Neutron Hydrogen Index, commonly named Neutron** (NHI, from the APS – Accelerator Porosity Sonde). A particular accelerator called a Minitron generates high energy neutrons (14 MeV) that are emitted into the formation. Elastic collisions with the atom nuclei slow down the neutrons, a process that is more efficient with nuclei whose mass is close to that of neutron, i.e., hydrogen (the lightest element). Five detectors count the neutrons back from the formation at different distances from the Minitron, allowing for an environmental compensation of the signal. The received signal is mostly (but not only, for example the chlorine atoms bring a significant contribution) dependent on the hydrogen concentration in the formation, hence the Hydrogen Index (HI) measurement: the larger the count, the lower the HI and its uncertainty. The APS tool can measure both an epithermal HI (APLC curve) and a thermal HI (FPLC). The hydrogen content in rocks is mostly in the fluids contained within, generally water or hydrocarbons, which have a HI close to 1 v/v. Nevertheless, some fluids like gas and high salinity brines have a HI lower than 1 v/v and must be corrected for when interpreting the results. In addition, many hydrated minerals are encountered in sedimentary or crystalline rocks, e.g. clay minerals, gypsum, iron-hydroxides, coals, zeolites, micas and amphiboles. The NHI is commonly used to quantify the fluid volume (porosity) and as a lithological indicator (clay content, hydrogen-rich minerals), mostly in combination with the bulk density measurement.
- **Resistivity** (HRLT – High Resolution Laterolog array Tool). The HRLT measures electrical resistivities at different depths of investigation in the formation. When drilling mud filtrate invades the formation and it has a salinity that contrasts with that of the formation fluids (the chlorine ion $Cl^-$ changes significantly the resistivity of a medium), the resistivities provide an invasion profile. Processing allows the extrapolation of the resistivity measurements far into the formation providing the true formation resistivity, as well as close to the tool providing the microresistivity or resistivity close to the borehole wall. Resistivity is used to interpret the saturation in water or hydrocarbons in pore spaces and for mineralogical identification (e.g. carbonates, clays, salt).
- **Sigma Formation Capture Cross-Section** (SIGF, from APS). In addition to the HI, the APS also measures the sigma formation capture cross-section (SIGF), that is defined as the relative ability of a material to "capture" or absorb free thermal neutrons. SIGF values vary widely with elements, and it can be used to determine the mineralogy and formation fluid contents.
- **Sonic** (MSIP – Modular Sonic Imaging Platform, also named Sonic Scanner). The MSIP measures how fast compressional and shear waves travel in the formation. A pulse sound is emitted from several tool transmitters in all directions. Tool receivers record the waves after they have travelled through a known path in the formation to the borehole wall. Waves travel at different velocities in the drilling fluid (between the tool and the borehole wall) and in the formation. Subtracting the travel time recorded by the near transmitter-receiver pairs from the

travel time recorded by far transmitter-receiver pairs provides the travel time spent in the formation only and thus discards the wave propagation in the fluid. Travel times are converted to wave slowness logs (inverse of velocity) based on the tool geometry. Compressional and shear wave slowness are used to interpret porosity, aid in mineralogy determination, for geomechanical and rock strength properties and they serve as calibration for seismic surveys. Other wave propagation such as flexural waves can be used to analyse the acoustic shear anisotropy properties of the formation. The MSIP log products require processing of the raw data to detect the different wave arrivals and transform the multiple transmitter-receiver recordings into unique slowness logs. Field processing products are basic and advanced processing products, such as the anisotropy analysis can be requested at a later stage.

- **Spectral Gamma Ray** (SGR, from the HNGS – Hostile Natural Gamma Ray Sonde). In addition to the total gamma ray, the HNGS measures the energy spectrum of the formation gamma rays. As the three main radioactive elements (potassium, thorium and uranium) are characterised by a different gamma energy, the tool can quantify those elements' content. Those concentrations can be used to quantify potassium-, uranium- or thorium-rich minerals (e.g. different clay minerals, potassic feldspars, organic matter, phosphates). The HSGR log is the sum of potassium, thorium and uranium gamma ray contributions to the total spectral gamma ray. Note that the total gamma ray from the GR and SGR tools are not necessarily quantitatively equivalent because these tools use different detectors, technologies, tool housing and calibrations. The HCGR log is the result of the HSGR log without the uranium contribution. The shading from HCGR to HSGR in log plots helps identify zones that may contain uranium-bearing organic matter and phosphates.
- **Spontaneous Potential** (SP). The SP log is a continuous measurement of the electric potential difference between an electrode in the SP tool and a surface electrode. Adjacent to shales, SP readings usually define a straight line known as the shale baseline. Next to permeable formations, the curve departs from the shale baseline; in thick permeable beds, these excursions reach a constant departure from the shale baseline, defining the "sand line". The deflection may be either to the left (negative) or to the right (positive), depending on the relative salinities of the formation water and the mud filtrate. If the formation water salinity is greater than the mud filtrate salinity (the more common case), the deflection is to the left. The movement of ions, essential to develop an SP, is possible only in rocks with some permeability, a small fraction of a millidarcy is sufficient. There is no direct relationship between the magnitude of the SP deflection and the formation's permeability or porosity.
- **Temperature** (TMP). The temperature log is acquired with the EMS tool that includes a temperature sensor. It is a measurement of the temperature in the borehole environment; thus, it is largely influenced by the temperature of mud. Since the temperature is affected by material outside the casing, a temperature log is sensitive to not only the borehole but also the formation and the casing – formation annulus. Mud temperature is generally less than that of fluids in the formation, but the temperature of the static mud is assumed to converge to the formation temperature after an infinite time. In practice, temperature logs are acquired several times after the last mud circulation, and the formation temperature is modelled based on the observed trend of temperature vs. time at each depth. On one hand, the temperature log is interpreted by looking for larger scale anomalies, or departures, from a reference gradient. This can give indications for permeable zones with fluid flow or for flow barriers hindering cross formational flow. On the other hand, localised smaller scale anomalies may correspond to the entry of borehole mud in the formation or fluid flow from the formation to the borehole. The temperature log should be interpreted together with structural geology, hydrogeology, and the other logs (e.g. images, resistivity logs).

## 3.2 Log data quality

### 3.2.1 Quality control procedures

Quality control (QC) of log data is important to guarantee their accuracy, repeatability, traceability, relevance, completeness, sufficiency, interpretability, clarity and accessibility. The generic QC procedures that were followed for each log dataset are presented as follows:

1. Digital data in .dlis format are loaded into a petrophysics software (Paradigm – Geolog) and checked for completeness (Are principal log channels, parameters and constants given?) and accessibility (Do the data load correctly when imported? Is the depth sampling rate steady and valid?).
2. Sufficient data: Do the first and last readings correspond to the interval of logs laid-out in the work programme?
3. Depth match is checked: main pass (or downlog pass if first run in hole) versus reference run, repeat pass(es) versus reference run. GR log of the EDTC tool is always used for correlation because it has excellent vertical resolution and sufficient character. Schlumberger depth matches data in the field, but sometimes additional depth-matching is required during QC. Such depth shifts are recorded in App. A8 – Table of post-acquisition depth shifts.
4. Are the calipers well calibrated? This is checked by comparing caliper measurements against the nominal inner diameter of the casing.
5. Borehole shape is checked: Are there washouts? Is the borehole on gauge? Undergauge? Ovalised? Are there breakouts? Hole restrictions? If the borehole shape is not gauge, the log quality can be degraded.
6. Cable tension is checked: does the cable tension show any overpulls or stick and pull events? These events can cause a locally discontinuous depth log measurement and alter the tool positioning which impacts the log quality. The tension log is also used to check that the logger depth is consistent with the tension pick-up.
7. Graphic files (log plots) are checked for completeness, consistency and accuracy. In particular, the following sections of the graphic files are checked:
   - 7.1 Header: e.g. logging date, run number, mud parameters
   - 7.2 Borehole sketch and size / casing record: hole bit sizes and depths, casing sizes, weight and depth
   - 7.3 Borehole fluids: accuracy of mud physical parameters
   - 7.4 Remarks and equipment summary: serial numbers of equipment, completeness and accuracy of remarks
   - 7.5 Depth control parameters: right depth control procedure and log of reference
   - 7.6 Summary of run passes: top and bottom of pass, automatic bulk shift applied
   - 7.7 Log (content and display): mnemonics, description, unit, scale, colour and label of logs; display of logs, log quality control (LQC) or data copy indicator curves provided (if applicable)
   - 7.8 Channel processing parameters, tool control parameters: corrections or offsets applied to measurements, modes of acquisition etc.
   - 7.9 Accelerometer and magnetometer crossplots provided (if applicable)
   - 7.10 Calibration reports: validity of master calibration and before calibration (if applicable), all calibrations within tolerances

8. Data repeatability for main vs. repeat passes (or downlog pass if applicable) is checked for a selection of important logs.
9. Were required, environmental corrections applied with the correct parameter values (e.g. mud salinity, mud weight, drill bit size, tool standoff, pressure / temperature).
10. Were processing parameters correctly applied (e.g. ECS minerals model options, MSIP time windows, APS lithology conversions)?
11. Data consistency is checked, including a comparison with logs from other runs via log plot and crossplots and the description of the cuttings for lithology. Are logs representative of expected lithologies and do they respond consistently?
12. Are orientation, accelerometer and magnetometer data accurate? This is essential for all data-sets that need to be oriented (e.g. borehole imagery [FMI/UBI], dipole sonic).
13. Mud resistivity and borehole temperature are checked for repeatability and checked against collected mud samples and thermometers in the logging head.
14. Quality of automatic picking on processing products (if applicable), e.g. compressional and shear wave slowness picking on semblance projections for sonic logs.

### 3.2.2 Bad-hole flags

To complete the data QC process, bad-hole flags were created to highlight zones where the log quality was degraded by 'bad-hole' conditions and should be viewed with caution. The methodology is presented in Tab. 3-1 and explained in detail in Appendix A7 – Badhole & unfit data flags.

Bad hole is a common issue with logging. It means that the borehole conditions are inadequate for obtaining optimum quality petrophysical logs that truly represent the formation that is being logged. The tools that either measure petrophysical properties in a space volume or must be in continuous contact with the borehole wall during logging (eccentered tools) are the most affected by bad hole. Washouts and rugose hole are the most common features that degrade the quality of the logs resulting for example in the underestimation of density and overestimation of sonic slowness.

Tab. 3-1: Bad-hole flag methodology

| **Bad-hole logic** | **Logs used** | **Cutoff/method** |
|---|---|---|
| Overgauge flag | Caliper | Borehole diameter is greater than 115% of nominal drill bit size |
| Rugosity flag | Density correction (HDRA), acquired with TLD | The density correction log is calculated from the difference between the short- and long-spaced density measurements, an indicator of borehole rugosity and density quality. Density is not reliable when HDRA > 0.025 g/cm$^3$ |
| Neutron standoff | Neutron standoff (STOF), acquired with APS | Neutron tool should be flushed with borehole wall or should have pre-determined physical standoff. If unintentional standoff, STOF > 0.35", bad hole is flagged |
| Density-neutron flag | Density (RHOZ) and neutron (APLC) | Systematic identification of outliers in density-neutron crossplot and comparison with analogue data from adjacent boreholes |

## 3.3 Composite log generation

The objective of the composite log dataset is to provide a traceable quality-controlled, edited, corrected and merged dataset for all petrophysical logging data recorded across the entire length of the borehole. Petrophysical tools acquire many logs that are not directly related to petrophysical properties but are needed to control that the tool sensors worked well (e.g. mechanical or electronics status of the sensors). In addition, some logs are acquired several times in a section (e.g. GR, Temperature). Ad Terra selects a collection of the most relevant logs for formation evaluation, correlation and calibration with core or seismic data. Some 107 representative logs are thus extracted for each borehole section. These logs are:

1. quality controlled (procedures in Section 3.2.1)
2. edited e.g. to keep data points that are true responses of the borehole and formation environment
3. further corrected for the borehole environment or artefacts
4. merged into composite logs that cover the entire or most of the borehole
5. The generated composite log dataset is generated and delivered in standard digital (LAS – Log ASCII Standard) and graphic (PDF log plot) format.

A more detailed procedure for the generation of the composite log is detailed in the next subchapter. In addition, a complete report in Excel format is provided (see Appendix A) which details all relevant information about the logs and the acquisition runs. Appendix A5 – Composite log generation worksheet specifically details how the composite log dataset was generated through merging techniques.

### 3.3.1 Generic process

The following steps were conducted to generate composite log dataset:

1. A bit size log was generated according to the borehole design at the time of logging (see Appendix A2 – Borehole design).
2. Logs were depth-shifted as required (see Appendix A8 – Post-acquisition depth shifts).
3. First and last readings were edited to remove values acquired before the tool sensors started reading the borehole (e.g. constant values just before/after the sensor is switched off/on) and/or before the tools started to move upward (e.g. stationary measurements close to total depth). Log readings were further edited if they did not read the borehole formation environment, e.g. logs can be impacted by the nearby casing shoe and cement, become decentralised when there are changes in the borehole diameter, or sediment infills at bottom of the borehole.
4. All logs that were not valid in cased hole were discarded. For the STA2-1 composite log dataset, this included all logs except for the total gamma ray log (ECGR_EDTC) from the EDTC and borehole temperature (TMP) from the EMS.
5. Bad-hole flags were created based on advanced log analysis to highlight zones where the log quality was affected by bad-hole conditions.
6. Total gamma ray log (ECGR_EDTC) was corrected for the radioactive potassium silicate in the drilling mud using the borehole potassium corrected total spectral gamma ray log (HSGR) for calibration. It was further normalised to account for attenuated readings in cased hole intervals according to standard practice. The corrected gamma ray log was then renamed GR_KCOR.
7. Poor quality sonic slowness data (DTCO, DTSM) caused by imprecise automatic picking were removed and interpolated where applicable.
8. The edited and corrected logs from each section were merged. Merging points were chosen carefully to optimise log coverage and composite log consistency. See Appendix A5 – Composite log generation.
9. Standardised log names, units and descriptions were used.
10. Logs acquired at higher resolution (e.g. RHO8, PEF8 have sample rates 0.0508 m – ⅙ ft) were resampled to the standard rate of 0.1524 m (½ ft), because the digital LAS format cannot support mixed sample rates.
11. Final log plots at a scale of 1:200 m MD, 1:1'000 m MD and 1:2000 m MD were produced in PDF graphic file format along with digital data in LAS format.

The composite Excel report and log plots at a scale of 1:200 m and 1:1'000 m MD and TVD can be found in Appendix A, Appendix B and Appendix C, respectively. Tab. 3-2 lists and describes all the log curves / channels that are provided in the composite log set.

Tab. 3-2: Composite log LAS channel listing

| **Curve / channel** | **Units** | **Description** |
|---|---|---|
| DEPTH | M | |
| APLC | V/V | Near/array Corrected Limestone Porosity (Epithermal HI) |
| BS | IN | Bit Size |
| DEVI | DEG | Borehole deviation |
| DTCO | US/F | Delta-T Compressional |
| DTSM | US/F | Delta-T Shear |
| DWAL_ALKNA | W/W | Dry Weight Fraction Pseudo Aluminium (SpectroLith ALKNA Model) |
| DWAL_MGWALK | W/W | Dry Weight Fraction Pseudo Aluminium (SpectroLith MWGALK Model) |
| DWAL_WALK2 | W/W | Dry Weight Fraction Pseudo Aluminium (SpectroLith WALK2 Model) |
| DWCA_ALKNA | W/W | Dry Weight Fraction Calcium (SpectroLith ALKNA Model) |
| DWCA_MGWALK | W/W | Dry Weight Fraction Calcium (SpectroLith MGWALK Model) |
| DWCA_WALK2 | W/W | Dry Weight Fraction Calcium (SpectroLith WALK2 Model) |
| DWCL_ALKNA | W/W | Dry Weight Fraction Chlorine Associated with Salt (SpectroLith ALKNA Model) |
| DWCL_MGWALK | W/W | Dry Weight Fraction Chlorine Associated with Salt (SpectroLith MGWALK Model) |
| DWCL_WALK2 | W/W | Dry Weight Fraction Chlorine Associated with Salt (SpectroLith WALK2 Model) |
| DWFE_ALKNA | W/W | Dry Weight Fraction Iron + 0.14 Aluminium (SpectroLith ALKNA Model) |
| DWFE_MGWALK | W/W | Dry Weight Fraction Iron + 0.14 Aluminum (SpectroLith MGWALK Model) |
| DWFE_WALK2 | W/W | Dry Weight Fraction Iron + 0.14 Aluminium (SpectroLith WALK2 Model) |
| DWGD_ALKNA | PPM | Dry Weight Fraction Gadolinium (SpectroLith ALKNA Model) |
| DWGD_MGWALK | PPM | Dry Weight Fraction Gadolinium (SpectroLith MGWALK Model) |
| DWGD_WALK2 | PPM | Dry Weight Fraction Gadolinium (SpectroLith WALK2 Model) |
| DWHY_ALKNA | W/W | Dry Weight Fraction Hydrogen Associated with Coal (SpectroLith ALKNA Model) |
| DWHY_MGWALK | W/W | Dry Weight Fraction Hydrogen Associated with Coal (SpectroLith MGWALK Model) |
| DWHY_WALK2 | W/W | Dry Weight Fraction Hydrogen Associated with Coal (SpectroLith WALK2 Model) |
| DWK_ALKNA | W/W | Dry Weight Fraction Potassium (SpectroLith ALKNA Model) |
| DWK_MGWALK | W/W | Dry Weight Fraction Potassium (SpectroLith MGWALK Model) |
| DWMG_MGWALK | W/W | Dry Weight Fraction Magnesium (SpectroLith MGWALK Model) |
| DWSI_ALKNA | W/W | Dry Weight Fraction Silicon (SpectroLith ALKNA Model) |
| DWSI_MGWALK | W/W | Dry Weight Fraction Silicon (SpectroLith MGWALK Model) |
| DWSI_WALK2 | W/W | Dry Weight Fraction Silicon (SpectroLith WALK2 Model) |

Tab. 3-2: continued

| **Curve / channel** | **Units** | **Description** |
|---|---|---|
| DWSU_ALKNA | W/W | Dry Weight Fraction Sulphur (SpectroLith ALKNA Model) |
| DWSU_MGWALK | W/W | Dry Weight Fraction Sulphur (SpectroLith MGWALK Model) |
| DWSU_WALK2 | W/W | Dry Weight Fraction Sulphur (SpectroLith WALK2 Model) |
| DWTI_ALKNA | W/W | Dry Weight Fraction Titanium (SpectroLith ALKNA Model) |
| DWTI_MGWALK | W/W | Dry Weight Fraction Titanium (SpectroLith MGWALK Model) |
| DWTI_WALK2 | W/W | Dry Weight Fraction Titanium (SpectroLith WALK2 Model) |
| FLAG_BADHOLE_OVERGAUGE | | Overgauge Borehole Bad-Hole Flag |
| FLAG_BADHOLE_RUGO | | Rugose Borehole Bad-Hole Flag |
| FLAG_BADHOLE_STOF | | Neutron Porosity Standoff Bad-Hole Flag |
| FLAG_UNFIT_ND | | Flag that indicates unfit neutron-density data for deterministic log evaluation |
| FPLC | V/V | Near/Far Corrected Limestone Porosity (Thermal HI) |
| GR_KCOR | GAPI | Total natural radioactivity corrected for the borehole potassium (EDTC) |
| HAZI | DEG | Borehole azimuth |
| HCGR | GAPI | HNGS Computed Gamma Ray |
| HDAR | IN | Hole Diameter from Area |
| HDRA | G/C3 | Density Standoff Correction |
| HFK | % | HNGS Formation Potassium Concentration |
| HSGR | GAPI | HNGS Standard Gamma-Ray |
| HTHO | PPM | HNGS Formation Thorium Concentration |
| HURA | PPM | HNGS Formation Uranium Concentration |
| PEF8 | B/E | High Resolution Formation Photoelectric Factor |
| PEFZ | B/E | Standard Resolution Formation Photoelectric Factor |
| RD1 | IN | Radius 1 |
| RD2 | IN | Radius 2 |
| RD3 | IN | Radius 3 |
| RD4 | IN | Radius 4 |
| RD5 | IN | Radius 5 |
| RD6 | IN | Radius 6 |
| RHGE_ALKNA* | G/C3 | Matrix Density from Elemental Concentrations (SpectroLith ALKNA Model) |
| RHGE_MGWALK* | G/C3 | Matrix Density from Elemental Concentrations (SpectroLith MGWALK Model) |
| RHGE_WALK2* | G/C3 | Matrix Density from Elemental Concentrations (SpectroLith WALK2 Model) |
| RHO8 | G/C3 | High Resolution Formation Density |
| RHOZ | G/C3 | Standard Resolution Formation Density |
| RLA0 | OHMM | Apparent Resistivity from Computed Focusing Mode 0 |
| RLA1 | OHMM | Apparent Resistivity from Computed Focusing Mode 1 |

Tab. 3-2: continued

| **Curve / channel** | **Units** | **Description** |
|---|---|---|
| RLA2 | OHMM | Apparent Resistivity from Computed Focusing Mode 2 |
| RLA3 | OHMM | Apparent Resistivity from Computed Focusing Mode 3 |
| RLA4 | OHMM | Apparent Resistivity from Computed Focusing Mode 4 |
| RLA5 | OHMM | Apparent Resistivity from Computed Focusing Mode 5 |
| RT_HRLT | OHMM | HRLT True Formation Resistivity |
| RXO8 | OHMM | Invaded Formation Resistivity filtered at 8 inches |
| RXOZ | OHMM | Invaded Formation Resistivity filtered at 18 inches |
| RXO_HRLT | OHMM | HRLT Invaded Zone Resistivity |
| SIGF | CU | Formation Capture Cross-Section |
| SP | MV | Spontaneous Potential |
| STOF | IN | Effective Standoff in Limestone |
| STPC | V/V | Corrected Standoff Porosity |
| SV | MPa | Overburden vertical stress (Sv) |
| TMP | DEGC | Mud Temperature at the time of logging |
| U8 | B/C3 | High Resolution Volumetric Photoelectric Factor |
| UZ | B/C3 | Volumetric Photoelectric Factor |
| WANH_ALKNA * | W/W | Dry Weight Fraction Anhydrite / Gypsum (SpectroLith ALKNA Model) |
| WANH_MGWALK * | W/W | Dry Weight Fraction Anhydrite/Gypsum (SpectroLith MGWALK Model) |
| WANH_WALK2 * | W/W | Dry Weight Fraction Anhydrite / Gypsum (SpectroLith WALK2 Model) |
| WCAR_ALKNA * | W/W | Dry Weight Fraction Carbonate (SpectroLith ALKNA Model) |
| WCAR_MGWALK * | W/W | Dry Weight Fraction Carbonate (SpectroLith MGWALK Model) |
| WCAR_WALK2 * | W/W | Dry Weight Fraction Carbonate (SpectroLith WALK2 Model) |
| WCLA_ALKNA * | W/W | Dry Weight Fraction Clay (SpectroLith ALKNA Model) |
| WCLA_MGWALK * | W/W | Dry Weight Fraction Clay (SpectroLith MGWALK Model) |
| WCLA_WALK2 * | W/W | Dry Weight Fraction Clay (SpectroLith WALK2 Model) |
| WCLC_MGWALK * | W/W | Dry Weight Fraction Calcite (SpectroLith MGWALK Model) |
| WCOA_ALKNA * | W/W | Dry Weight Fraction Coal (SpectroLith ALKNA Model) |
| WCOA_MGWALK * | W/W | Dry Weight Fraction Coal (SpectroLith MGWALK Model) |
| WCOA_WALK2 * | W/W | Dry Weight Fraction Coal (SpectroLith WALK2 Model) |
| WDOL_MGWALK * | W/W | Dry Weight Fraction Dolomite (SpectroLith MGWALK Model) |
| WEVA_ALKNA * | W/W | Dry Weight Fraction Salt (SpectroLith ALKNA Model) |
| WEVA_WALK2 * | W/W | Dry Weight Fraction Salt (SpectroLith WALK2 Model) |
| WPYR_ALKNA * | W/W | Dry Weight Fraction Pyrite (SpectroLith ALKNA Model) |
| WPYR_MGWALK * | W/W | Dry Weight Fraction Pyrite (SpectroLith MGWALK Model) |
| WPYR_WALK2 * | W/W | Dry Weight Fraction Pyrite (SpectroLith WALK2 Model) |

Tab. 3-2: continued

| Curve / channel | Units | Description |
|---|---|---|
| WQFM_ALKNA * | W/W | Dry Weight Fraction Quartz+Feldspar+Mica (QFM) (SpectroLith ALKNA Model) |
| WQFM_MGWALK * | W/W | Dry Weight Fraction Quartz+Feldspar+Mica (QFM) (SpectroLith MGWALK Model) |
| WQFM_WALK2 * | W/W | Dry Weight Fraction Quartz+Feldspar+Mica (QFM) (SpectroLith WALK2 Model) |
| WSID_ALKNA * | W/W | Dry Weight Fraction Siderite (SpectroLith ALKNA Model) |
| WSID_MGWALK * | W/W | Dry Weight Fraction Siderite (SpectroLith MGWALK Model) |
| WSID_WALK2 * | W/W | Dry Weight Fraction Siderite (SpectroLith WALK2 Model) |

* Qualitative data should only be used as a lithology indicator.

### 3.3.2 Gaps in log coverage

Optimising the petrophysical log and MHF testing coverage was an objective of the logging and testing campaigns, in particular for the potential Opalinus Clay rock host. Despite best efforts, gaps in log coverage are an inherent limitation in wireline logging operations.

Complete log coverage at changes in drilling section is possible if the acquisition of the lowermost part of the drilling section is repeated later with the acquisition of the uppermost part of the drilling section below. Logs acquired with the same sensor, which overlap over two sections can then be merged providing complete coverage. This is not always possible due to limitations related to tool string geometry, borehole conditions and borehole design. Examples include:

- Cuttings infill the bottom of the hole preventing the tool string from reaching total depth.
- The tool string should not tag the bottom hole with certain fragile tools (e.g. UBI).
- The offset of the sensors relative to the bottom of the tool string.
- The rathole clearance (space between casing shoe and the bottom of the drilled hole) available for logging in the section below is too short. If the casing shoe is too close to the bottom of the section and the lowermost part of the open hole was not logged before casing installation, some log coverage will be lost.
- The rathole available for logging in the section below is first enlarged, and its diameter is different (e.g. 12¼") from that of the cored section below (6⅜"). Abrupt changes in borehole size are not favourable for logging because they are often associated with bad hole and eccentered tools in contact with the borehole wall acquire logs of degraded quality, causing gaps in log coverage.

The above factors were taken into consideration in the design of work programmes. For each logging campaign, project guidelines defined the balance between the optimisation of log coverage (short tool strings, more runs, longer campaign) and saving rig time and associated costs (slightly longer tool strings, less runs, shorter campaign).

For the main drilling sections where petrophysical logs were acquired (Section II to TD), a summary of the meterage of logged data and the percentage of total depth this data represents, is summarised in Tab. 3-3. The Opalinus Clay and bounding formations (Dogger – Lias) were examined in greater detail. Almost complete log coverage was acquired in these formations.

Tab. 3-3: Summary of petrophysical log coverage from drilling Section II to TD

| **Measurement** | **Section II to TD** (470.00 m – 1'288.12 m MD) | | **Opalinus Clay and Bounding Formations (Dogger to Lias)** (728.20 m – 941.42 m MD) | |
|---|---|---|---|---|
| | **Meterage** [m] | **Coverage** [%] | **Meterage** [m] | **Coverage** [%] |
| Caliper | 815.03 | 99.6 | 213.22 | 100.0 |
| Borehole orientation | 813.70 | 99.5 | 212.15 | 99.5 |
| Total Gamma Ray | 812.45 | 99.3 | 213.22 | 100.0 |
| Spontaneous Potential | 811.71 | 99.2 | 213.22 | 100.0 |
| Spectral Gamma Ray | 811.42 | 99.2 | 210.21 | 98.6 |
| Density | 807.37 | 98.7 | 211.70 | 99.3 |
| Photoelectric Factor | 807.37 | 98.7 | 211.70 | 99.3 |
| Microresistivity | 805.69 | 98.5 | 211.70 | 99.3 |
| Neutron (NHI) | 804.22 | 98.3 | 209.26 | 98.1 |
| Sigma Formation Capture Cross-Section | 804.22 | 98.3 | 209.26 | 98.1 |
| Resistivity | 787.19 | 96.2 | 203.00 | 95.2 |
| Sonic | 808.79 | 98.9 | 213.22 | 100.0 |
| Element Spectroscopy | 813.36 | 99.4 | 211.54 | 99.2 |
| Ultrasonic Borehole Imagery | 577.50 | 70.6 | 213.22 | 100.0 |
| Microresistivity Borehole Imagery | 810.52 | 99.1 | 210.52 | 98.7 |

The depths at which there were gaps in log coverage in the final composite dataset are detailed in Appendix A5 – Composite log generation.

## 3.4 Petrophysical logging results and description

The main features of the petrophysical logs of the composite dataset are described below by litho-stratigraphic units.

### 3.4.1 Malm: «Felsenkalke» + «Massenkalk» to Wildegg Formation (433 to 728.20 m MD)

No valid logs except the caliper, total GR and sonic were acquired in Section I of the borehole. The top of the Malm («Felsenkalke» + «Massenkalk») can be identified by a decrease in total GR (GR_KCOR) and sonic (DTCO) (Fig. 3-1).

Log responses reflect the borehole lithology well, except for some short overgauge and rugose bad-hole zones in the rathole of Section I in the «Felsenkalke» + «Massenkalk» and in the upper Wildegg Formation, where the response of most logs was affected, including the neutron, density and sonic logs.

Logs in the Malm units have an overall similar log signature characterised by (Fig. 3-1):

- Generally low clay content in the «Felsenkalke» + «Massenkalk») and Villigen Formation: low total GR (GR_KCOR: 0 to 73 GAPI; mean = 13 GAPI), spectral GR (e.g. thorium HTHO: 0 to 7.6 ppm; mean = 1.2 ppm) and sigma (SIGF: 7.0 to 23.4 CU; mean = 10.5 CU). Clay content increases in the Schwarzbach Formation and the Wildegg Formation (GR_KCOR: 9 to 77 GAPI; mean = 39 GAPI).
- Calcite is the dominant mineral: an almost perfect overlap in the neutron-density limestone-compatible scale (density [RHOZ] and neutron [APLC] readings in pure limestone are 2.71 g/cm$^3$ and 0.0 v/v, respectively), the calcium dry weight fraction (DWCA) is close to that of pure calcite (0.394 W/W), as is the photoelectric factor (PEFZ) – pure calcite value of 5.1 B/E.
- In the low clay units (GR_KCOR < 25 GAPI), porosity is low, density is high (rarely lower than 2.64 g/cm$^3$; mean: 2.68 g/cm$^3$) and sonic (DTCO) rarely exceeds 68 µs/ft.
- The qualitative classification of clay minerals based on the spectral GR potassium (HFK) and thorium (HTHO) logs is not relevant given the low clay content.

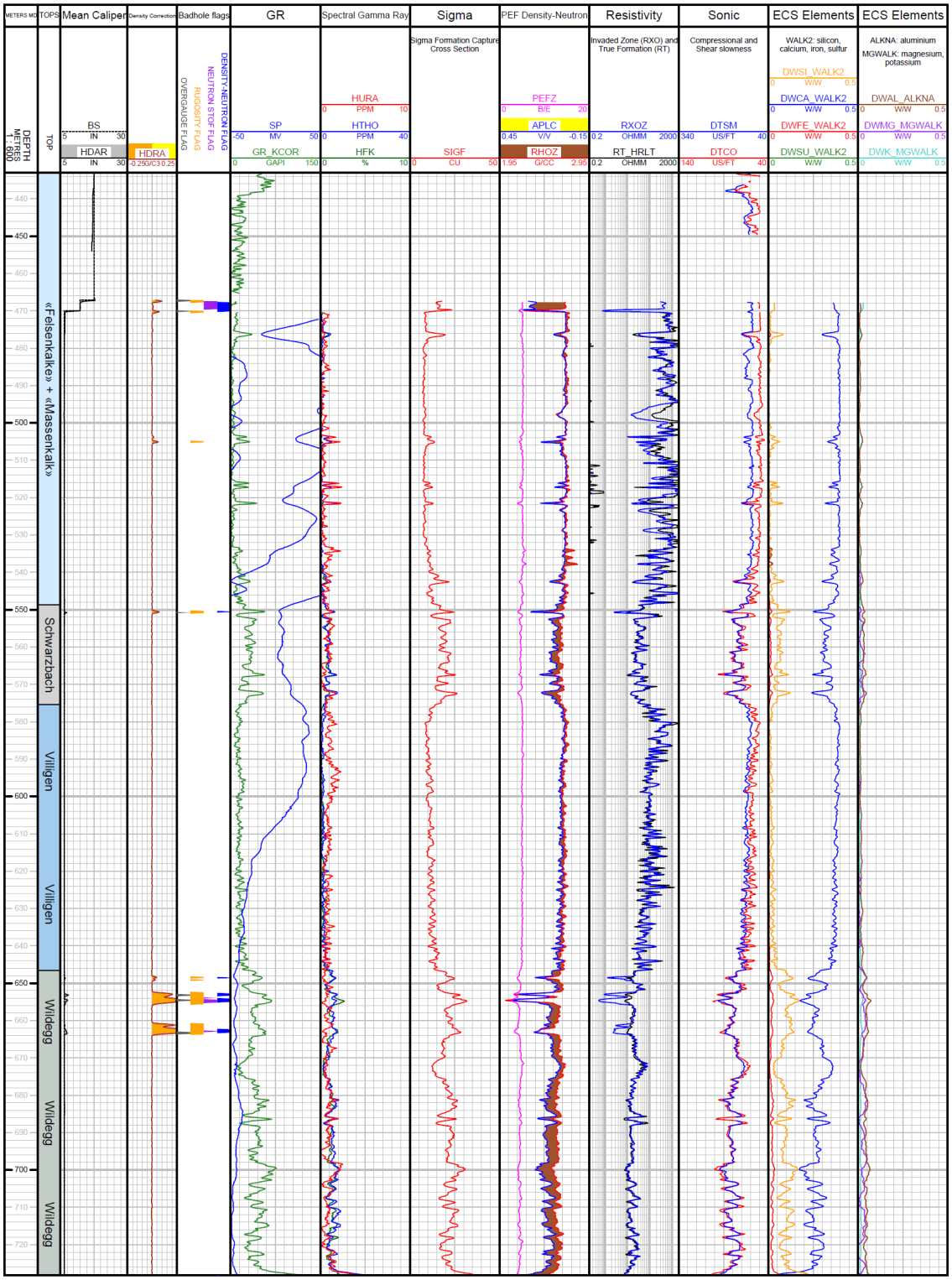


Fig. 3-1: Main logs of the composite dataset in the «Felsenkalke» + «Massenkalk» to Wildegg Formation

### 3.4.2 Wutach Formation to «Murchisonae-Oolith Formation» (728.20 to 800.67 m MD)

The top of the Dogger (Wutach Formation) can be identified by an increase in siderite, iron oxide or hydroxide bearing rocks indicators such as the ECS iron dry weight fraction (DWFE), a wide separation in the neutron-density logs (displayed in a limestone-compatible scale), and PEFZ (Fig. 3-2).

Due to good-hole conditions, log responses reflect the borehole lithology well from the Wutach Formation to the «Murchisonae-Oolith Formation». Logs have the following attributes:

- Low («Herrenwis Unit») to moderately high (Wutach Formation, Variansmergel Formation and «Parkinsoni-Württembergica-Schichten») total GR. Excluding the zones that contain siderite, iron oxides or hydroxides (DWFE > 0.075 W/W), GR_KCOR ranges from 16 to 117 GAPI, SIGF ranges from 11.8 to 41.7 CU and HTHO ranges from 2.0 to 16.4 ppm.
- The occurrence of siderite, iron oxide or hydroxide is typical in these formations: a wide separation in the density-neutron, high total and spectral GR (especially thorium HTHO up to 39.3 ppm and uranium HURA up to 7.9 ppm), high iron concentration (DWFE: above 0.075 W/W) and high photoelectric factor (PEFZ up to 9.4 B/E).
- The matrix mineralogy is dominated by calcite: in the lowest clay and low iron zones PEFZ is in the range of 3.5 to 6.2 B/E, while calcium is relatively high (DWCA: up to 0.33 W/W; 0.394 W/W in pure calcite), which is typical of limestones and marls. In parts of the «Herrenwis Unit», the separation between the neutron-density is almost absent, an indication that calcite is dominant. Conversely, quartz is the main matrix component in the Wedelsandstein Formation. This is indicated by the intermediate to high DWSI (mean = 0.23 W/W) and the absence of correlation between clay content and silicon, which shows that the silicon is not primarily related to the clays.
- The spectral GR potassium (HFK) and thorium (HTHO) logs suggest the presence of both non-potassic (e.g. kaolinite, smectite) and potassic (e.g. illite) clay minerals.

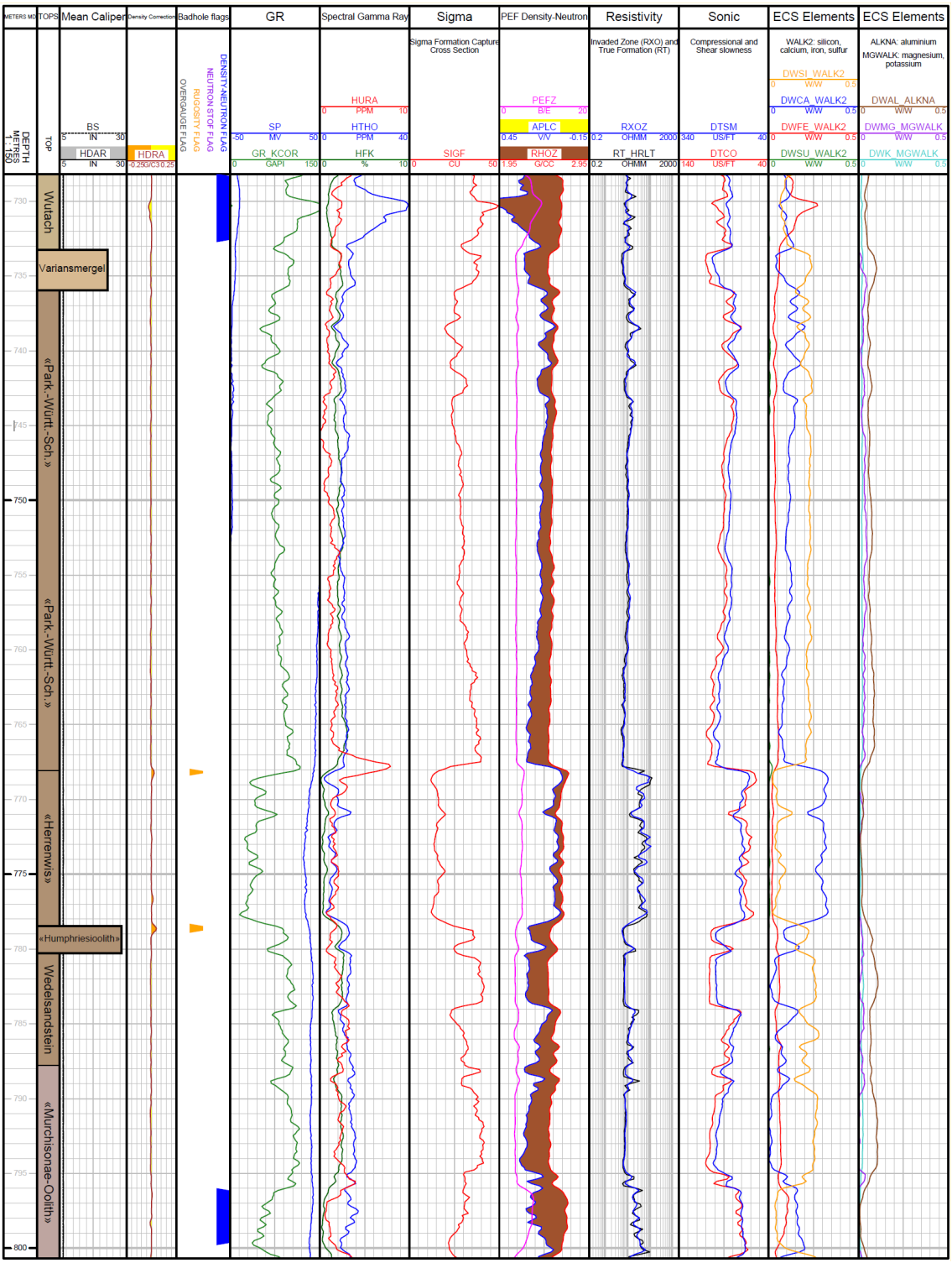


Fig. 3-2: Main logs of the composite dataset in the Wutach Formation to «Murchisonae-Oolith Formation»

### 3.4.3 Opalinus Clay (800.67 to 906.87 m MD)

The top Opalinus Clay is characterised by an increase in clay content, as observed by the increase in total GR (GR_KCOR) and sigma (SIGF) and decrease in calcium concentration (DWCA).

Log responses reflect the borehole lithology well because hole conditions were excellent for wireline logging. In the Opalinus Clay, logs have the following attributes (Fig. 3-3):

- Consistently intermediate to high clay content: the GR_KCOR ranges from 57 to 116 GAPI; SIGF correlates very well (positively) to GR_KCOR, ranging from 23.4 to 48.2 CU; the compressional wave slowness DTCO is high (slow formation) and generally above 87 µs/ft; the density-neutron separation is typical of lithologies with high clay content.
- Several carbonate streaks can be observed at 806.70, 816.20, 819.90 and 824.50 m MD characterised by: an increase in density and decrease in neutron with values approaching those of pure calcite (RHOZ: 2.71 g/cm$^3$; APLC: 0.0 v/v); an increase in calcium (DWCA up to 0.18 W/W); an increase in resistivity logs (e.g. RT_HRLT).
- While the clay content is relatively homogeneous throughout, two distinct trends can be observed. In the upper part of the formation, above 833.70 m MD, the clay content varies with carbonate content and generally remains lower than in the lower Opalinus Clay. Below 833.70 m MD, the clay content increases slightly with depth, as indicated by the gradual widening of the density-neutron separation and the increase in SIGF. Carbonate streaks are absent in the lower part of the formation.
- Matrix mineralogy is complex. Both calcium (DWCA) and silicon (DWSI) concentrations are often higher than those in non-potassic and potassic clays (DWCA: 0.00 W/W to 0.10 W/W; DWSI: 0.21 W/W to 0.30 W/W, excluding the carbonate streaks), which suggests siliciclastic and carbonate components in the matrix.
- The spectral GR potassium (HFK) and thorium (HTHO) logs suggest the presence of both non-potassic (e.g. kaolinite, smectite) and potassic (e.g. illite) clay minerals.

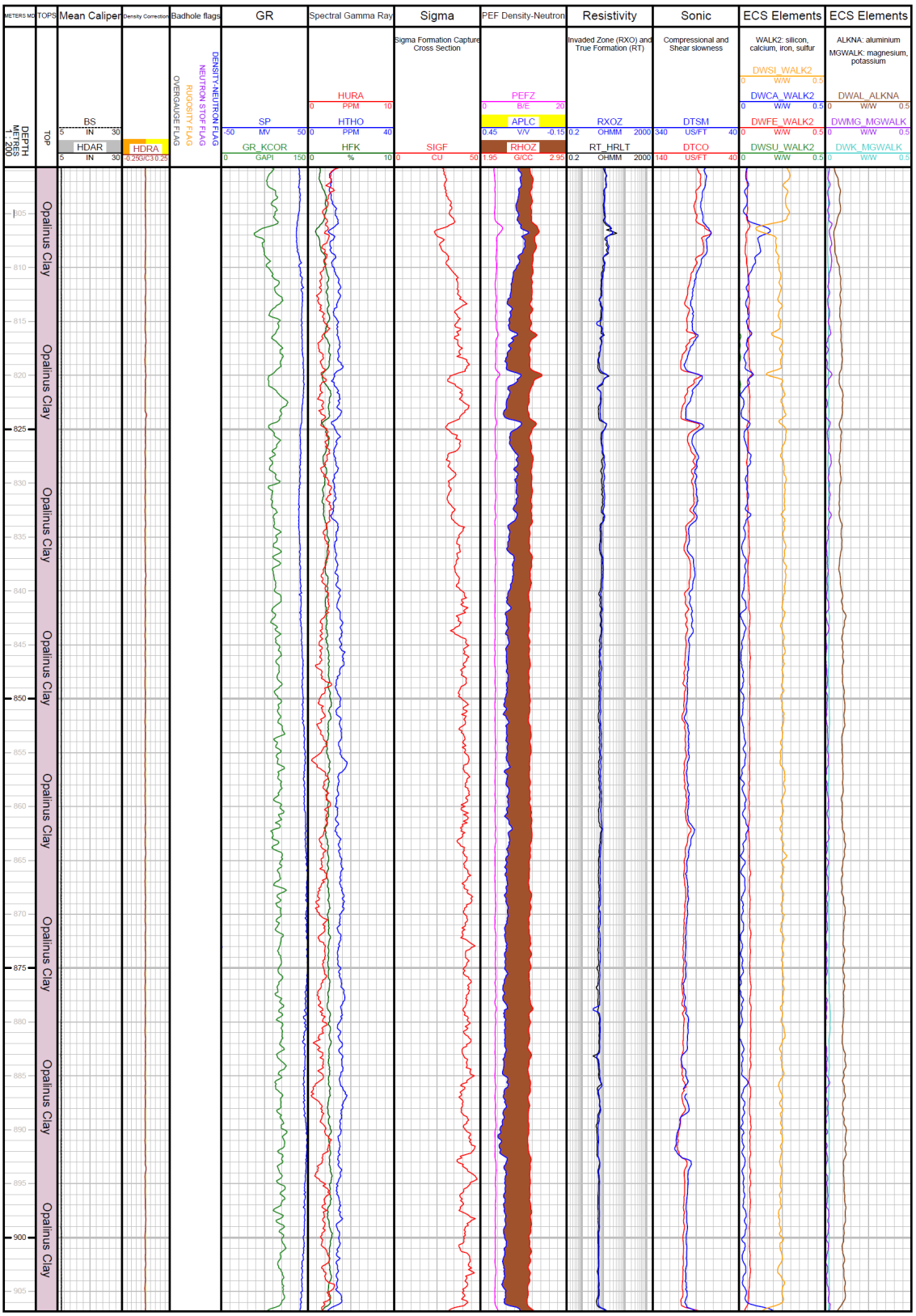


Fig. 3-3: Main logs of the composite dataset in the Opalinus Clay

### 3.4.4 Staffelegg Formation (906.87 to 941.42 m MD)

The top of the Lias (Staffelegg Formation) can be identified by a decrease in total GR (GR_KCOR) and sigma (SIGF), a narrower separation in the density-neutron logs in a limestone-compatible scale and an increase in calcium contents (DWCA) (Fig. 3-4).

Hole conditions were good in the Staffelegg Formation, except in the rathole of Section III in the Schambelen Member. Logs respond well to the borehole lithology having the following attributes:

- Highly variable clay content: total GR (46 to 235 GAPI, excluding the organic matter), sigma (17.7 to 47.4 CU) and thorium (2.9 to 17.0 ppm), e.g. low clay content in the Beggingen Member (931.82 to 934.76 m MD) but intermediate to high clay content in the Schambelen Member (934.76 to 941.42 m MD).
- Organic matter is likely present: the high total GR zones (GR_KCOR > 125 GAPI) correspond with the uranium peaks (HURA: up to 22.5 ppm) in the Grünschholz Member, Breitenmatt Member, Rickenbach Member and Beggingen Member.
- Pyrite is an important accessory mineral throughout the Staffelegg Formation: ECS sulphur dry weight fraction (DWSU) ranges from 0 to 0.03 W/W and the PEFZ, a reactive marker of pyrite, reaches a high value of 6.4 B/E.
- Matrix mineralogy is dominated by carbonate: calcium (DWCA) varies between 0 and 0.33 W/W (pure calcite: 0.394 W/W); however, mineralogy remains complex. The multi-mineral interpretation detailed in Dossier X will help to better understand this complex mineralogy.
- The spectral GR potassium (HFK) and thorium (HTHO) logs suggest the presence of both non-potassic (e.g. kaolinite, smectite) and potassic (e.g. illite) clay minerals.

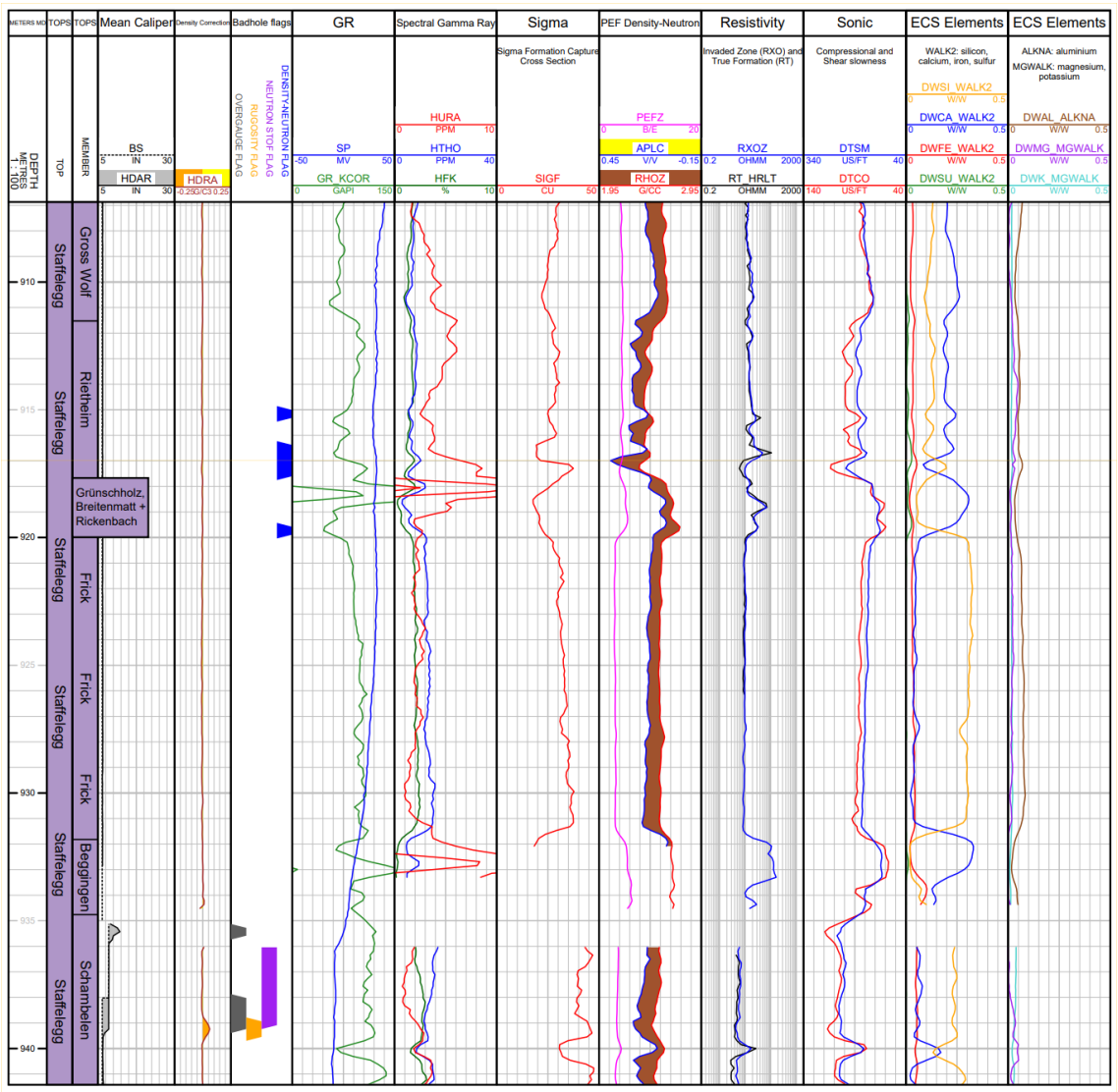


Fig. 3-4: Main logs of the composite dataset in the Staffelegg Formation

### 3.4.5 Klettgau Formation (941.42 to 970.52 m MD)

The top of the Klettgau Formation was identified from logs to be a gradual transition from 941.20 m MD to 942.40 m MD, where clay content decreases (e.g. GR_KCOR, HTHO, SIGF) and matrix mineralogy becomes more calcitic (DWCA increases).

Hole conditions were good in the Klettgau Formation. Logs respond well to the borehole lithology having the following attributes:

- Highly variable clay content: total GR ranges from ranges from 15 to 126 GAPI, sigma from 11.0 to 44.1 CU and thorium from 1.5 to 13.8 ppm; clay indicators have a bimodal distribution that reflects zones with low clay content (Seebi Member and Gansingen Member) and zones with moderately low to intermediate clay content (Gruhalde Member and Ergolz Member).
- Carbonate is the main matrix mineral in the Seebi Member and the Gansingen Member, as indicated by the intermediate to high calcium concentration (DWCA: 0.16 to 0.34 W/W; pure calcite: 0.394 W/W). The carbonate has a dolomitic signature, as shown by the photoelectric factor (PEFZ) whose mean value (3.7 B/E) is close to that of pure dolomite (3.1 B/E), and ECS magnesium concentration (DWMG: 0.07 to 0.11 W/W).
- In the Gruhalde Member, the calcium and silicon concentrations are intermediate (mean DWCA: 0.16 W/W; mean DWSI: 0.17 W/W) and they are only loosely correlated with the clay content, indicating a mixed matrix mineralogy.
- In the Ergolz Member, the calcium concentration is low (mean DWCA: 0.03 W/W) and the silicon concentration increases up to 0.33 W/W. This is also true for the zones with low clay content and suggests that the matrix mineralogy is dominated by siliciclastic minerals such as quartz. The density-neutron crossover below 963.70 m MD (density is to the left of neutron in the limestone-compatible scale: yellow shading) also supports the presence of quartz.
- Organic matter is likely present, particularly at the base of the formation: HURA increases up to 5.1 ppm.
- The spectral GR potassium (HFK) and thorium (HRHO) logs suggest the presence of both non-potassic (e.g. kaolinite, smectite) and potassic (e.g. illite) clay minerals in the clay-rich zones.

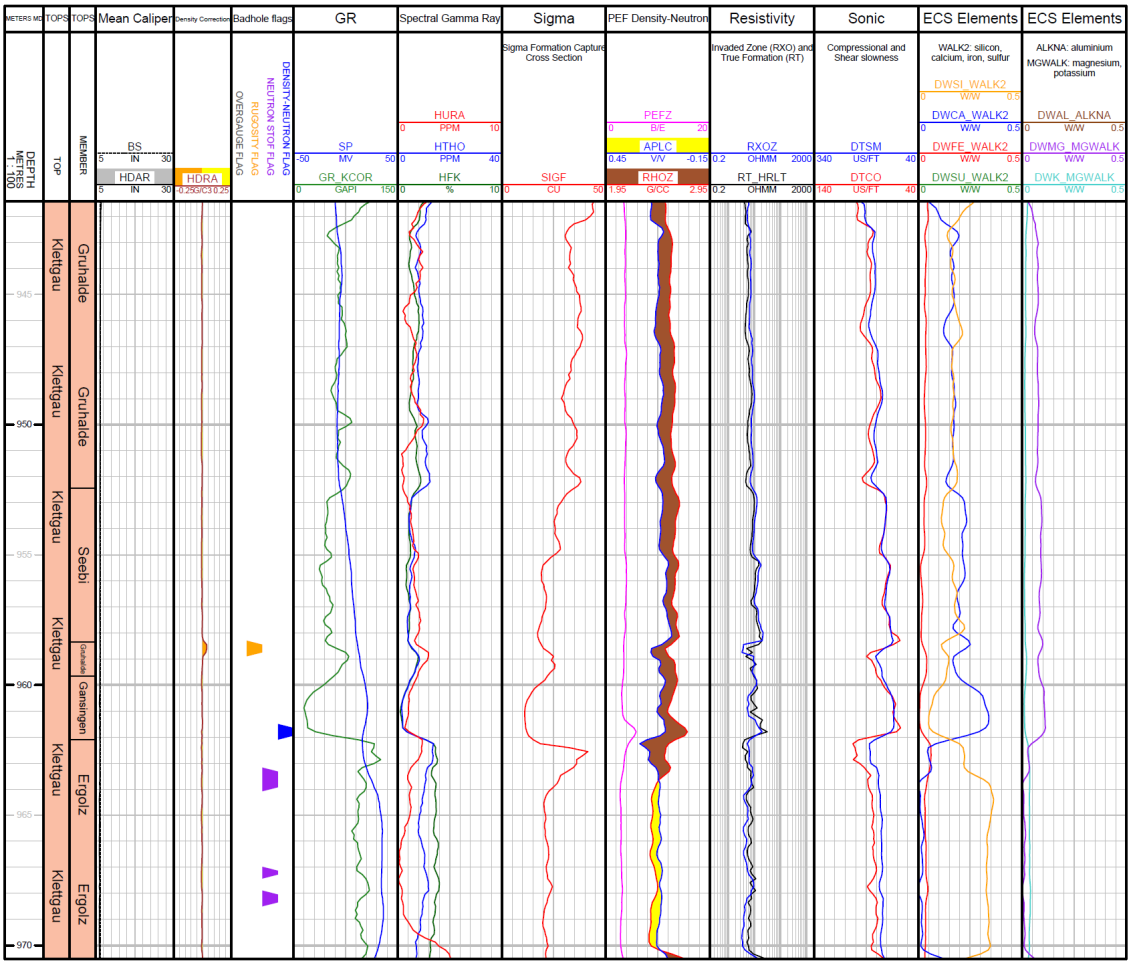


Fig. 3-5: Main logs of the composite dataset in the Klettgau Formation

### 3.4.6 Bänkerjoch Formation (970.52 to 1'043.62 m MD)

The top of the Bänkerjoch Formation is characterised by an increase in evaporite (DWSU) and clay content (GR_KCOR, density-neutron separation) and decrease in clastic content (DWSI), associated with the transition from the silty-dominated lithology of the Ergolz Member to the anhydrite/claystone deposits of the Bänkerjoch Formation.

Logs respond well to the lithology in this formation because hole conditions were good and are characterised by the following attributes (Fig. 3-6):

- Rapid variations in most logs at the metre scale or less from 993.40 m to 1'036.80 m MD, which suggest two main alternating lithologies. One having high sulphur (DWSU: up to 0.21 W/W) and calcium concentrations (DWCA: up to 0.34 W/W), high high photoelectric factor (PEFZ: up to 5.9 B/E) and intermediate to low total GR, which suggest predominantly anhydrite bearing beds. The alternate beds have a higher clay content as indicated by the lower sulphur and calcium concentrations, high DWSI (up to 0.23 W/W) and intermediate to high total GR.
- The density-neutron separation (displayed in the limestone-compatible scale) remains similar for both lithologies, but logs shift from left to right for the clay and anhydrite dominant end-members, respectively.
- Below 1'036.80 m MD, the lower Bänkerjoch Formation contains two massive anhydrite beds, as indicated by consistently high DWSU (up to 0.23 W/W) and DWCA (up to 0.33 W/W), while clay content indicators remain low (e.g. GR_KCOR).
- Due to the limited vertical resolution of the logging tool, often higher than 10" (e.g. APS: 14"), the alternating lithologies are not necessarily correctly reflected in the logs. The logging tools average the physical and chemical properties over a fixed volume, which means that centimetre scale beds are represented as a mixture of anhydrite and clays for a given depth.
- The spectral GR potassium (HFK) and thorium (HTHO) logs suggest the presence of both non-potassic (e.g. kaolinite, smectite) and potassic (e.g. illite) clay minerals in the clay-rich zones.

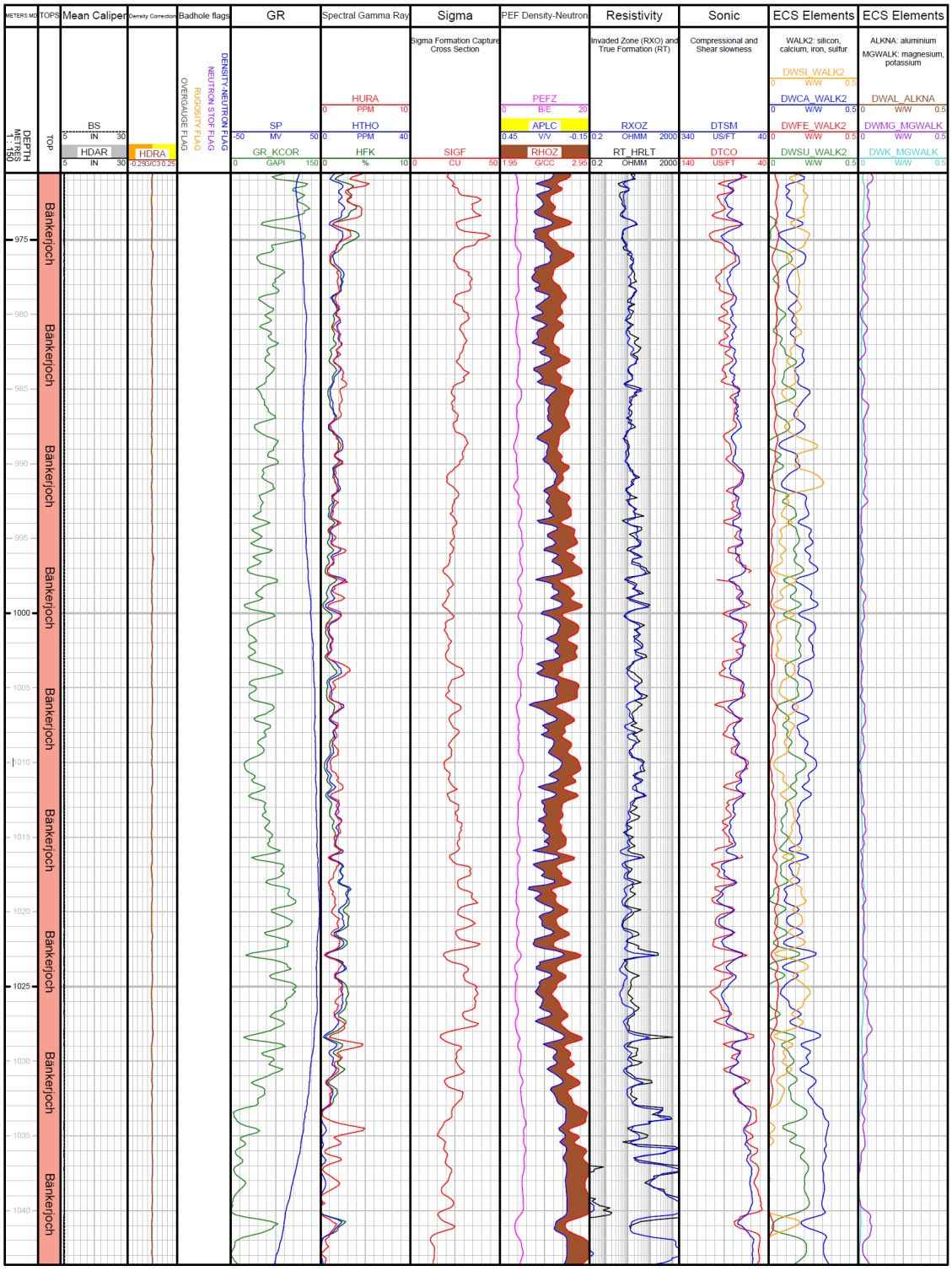


Fig. 3-6: Main logs of the composite dataset in the Bänkerjoch Formation

### 3.4.7 Schinznach Formation (1'043.62 to 1'116.69 m MD)

The top of the Schinznach Formation is identified by a decrease in the sulphur content (DWSU), the photoelectric factor (PEFZ) and sigma (SIGF) below the second massive anhydrite bed of the Bänkerjoch Formation.

Hole conditions were mostly good in the Schinznach Formation and logs responded well to the borehole lithology, except in the rathole below the 7⅝" liner. Logs in the Schinznach Formation are characterised by the following attributes (Fig. 3-7):

- Low to moderately low clay content as shown by the total GR (GR_KCOR: 10 to 60 GAPI), sigma (SIGF: 6.8 to 29.0 CU) and thorium (HTHO: 0 ppm to 4.7 ppm), except in the interval from 1'046.30 m to 1'048.30 m MD in the Asp Member where a clay-rich layer is present.
- Carbonate is the main matrix mineral as shown by the fast sonic (DTCO, DTSM), low silicon (DWSI) and high calcium concentrations (DWCA: up to 0.40 W/W; pure calcite is 0.394 W/W for comparison).
- From the top of the Schinznach Formation to 1'081.50 m MD, the carbonate has a dolomitic signature as shown by the photoelectric factor (PEFZ) whose mean value of 3.3 B/E is close to that of pure dolomite (3.1 B/E), whilst the density-neutron separation is positive, the DWMG is high (mean: 0.11 W/W) and the clay content is low. The large separation between the shallow (RXOZ) and deep (RT_HRLT) resistivities indicate invasion of mud filtrate into the permeable formation across several zones.
- From 1'081.50 m MD to the bottom of the Schinznach Formation, the mean PEFZ (4.5 B/E) is close to that of pure calcite (5.1 B/E) and the density-neutron separation is slightly positive or absent, suggesting that the carbonates are composed of limestones and dolomitic limestones.
- Anhydrite is present in the Asp Member and parts of the Stamberg, Leutschenberg and Kienberg Members, as indicated by the DWSU (up to 0.14 W/W).
- The qualitative classification of clay minerals based on the spectral GR potassium (HFK) and thorium (HTHO) logs is not relevant given the low clay content.

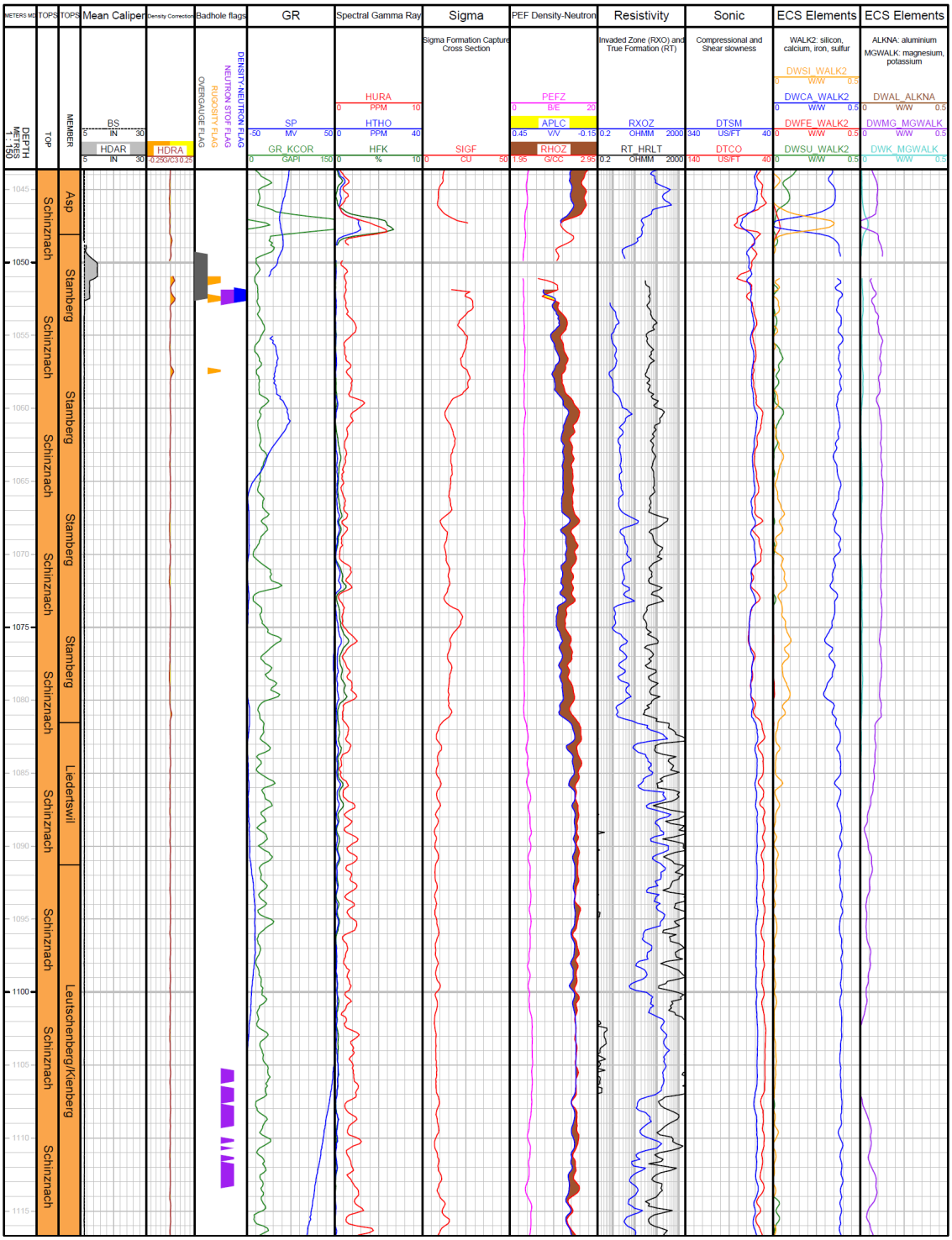


Fig. 3-7: Main logs of the composite dataset in the Schinznach Formation

### 3.4.8 Zeglingen Formation (1'116.69 to 1'185.42 m MD)

The top of the Zeglingen Formation corresponds to a decrease in calcium content (DWCA), an increase of silicon (DWSI) and magnesium (DWMG) contents and a slight decrease in the photo-electric factor (PEFZ) as the matrix minerology changes from calcite-dominated carbonate to dolostone.

Hole conditions were good except in the «Salzlager» (from 1'152.02 m to 1'179.58 m MD), where there were washouts and rugosity. Outside this zone, logs responded well to borehole lithology. The Zeglingen Formation is characterised by the following (Fig. 3-8):

- Low to moderately high clay content: total GR (GR_KCOR: 3 to 123 GAPI), sigma (SIGF: 2 to 49.9 CU) and thorium (HTHO: 0.1 to 8.0 ppm).
- Density (RHOZ) is often greater than 2.9 g/cm$^3$ suggesting the presence of massive or laminated anhydrite. This is supported by PEFZ that is close to the value of pure anhydrite (5.05 B/E) and the significant sulphur content (DWSU: up to 0.24 W/W; value in anhydrite: 0.236 W/W).
- From the top of the Zeglingen Formation to 1'134.50 m MD, logs indicate less anhydrite, and dolomite is the main mineral component as shown by the PEFZ values that are close to those of pure dolomite (3.1 B/E) and DWCA that ranges from 0.20 to 0.39 W/W.
- In the «Dolomitzone», the separation of laterolog resistivities at different depths of investigation suggests mud filtrate invasion and thus formation permeability. This separation is more pronounced in the low-clay, porous dolomitic interval close to the top of the unit.
- The «Salzlager» is characterised by very low densities (RHOZ: lower than 2.45 g/cm$^3$) and very high sigma (SIGF: up to 50 CU), which are typical for salt deposits.
- The spectral GR potassium (HFK) and thorium (HTHO) logs suggest the presence of both non-potassic (e.g. kaolinite, smectite) and potassic (e.g. illite) clay minerals in the clay-rich zones.

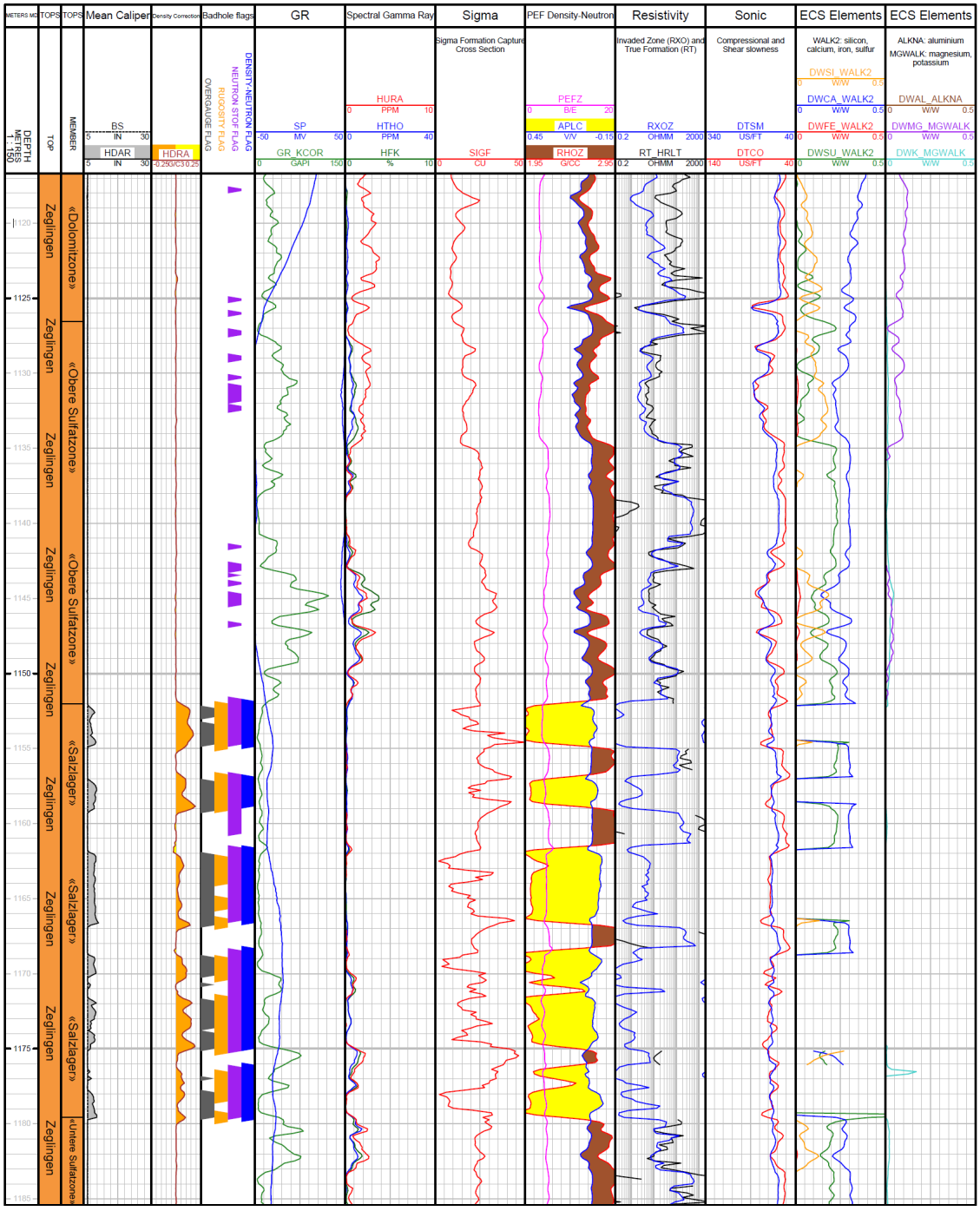


Fig. 3-8: Main logs of the composite dataset in the Zeglingen Formation

### 3.4.9 Kaiseraugst Formation (1'185.42 m to 1'225.07 m MD)

The top of the Kaisergaust Formation is defined as the base of the last massive anhydrite bed of the overlying Zeglingen Formation. It is thus characterised by a decrease in the sulphur content (DWSU). In addition, the clay content markers slightly increase: total GR (GR_KCOR), silicon content (DWSI) and thorium (HTHO).

Due to the good-hole conditions, log responses reflect the borehole lithology well (Fig. 3-9). Logs in the Kaiseraugst Formation have the following attributes:

- Low to moderately high clay content as shown by the total GR (GR_KCOR: 12 to 165 GAPI), sigma (SIGF: 13.7 to 37.2 CU) and thorium (HTHO: 0.5 to 16.5 ppm). The anhydrite-rich «Orbicularismergel» contains little clay, as does the bottom part of the «Wellendolomit» which contains siliciclastics. The «Wellenmergel» has the highest clay content. The unusually high values shown by the clay indicators in the argillaceous marlstones described by the wellsite geologists are likely due to the presence of bituminous shales (described in Jordan 2016). Gas while drilling supports this theory as total gas measurements showed a slight increase (< 1%). Core measurements will allow a better understanding of the rock components.
- The anhydrite beds in the «Obricularismergel» are characterised by their high sulphur content (DWSU: up to 0.22 W/W; pure anhydrite: 0.236 W/W), low total GR (GR_KCOR: mean = 30 GAPI) and high resistivities (e.g. RT_HRLT).
- The «Wellendolomit» below 1'221.80 m MD contains predominantly siliciclastics (e.g. quartz) as indicated by an increase in DWSI. However, the PEFZ never records values below 2.6 B/E, implying that the matrix also contains carbonates (pure quartz: 1.8 B/E; pure dolomite: 3.1 B/E; pure calcite: 5.1 B/E).
- Below the last anhydrite layer (1'194.20 m MD) to the upper part of the «Wellendolomit» (1'221.80 m MD), logs show relatively homogeneous values, e.g. an intermediate density-neutron separation, intermediate sonic (90% of DTCO values ranged from 76 µs/ft to 99 µs/ft) and consistent iron concentrations (DWFE: 0.02 to 0.06 W/W). These data suggest intermediate to moderately high clay content as is common in marlstone.
- Excluding the anhydrite layers, the DWSI ranges from 0.09 W/W to 0.35 W/W with a mean of 0.22 W/W, whereas the DWCA is only 0.11 W/W. PEFZ also remains lower than the pure calcite value of 5.1 B/E, ranging from 3.0 B/E to 4.8 B/E, suggesting that dolomite is also a matrix component.
- Clay minerals could not be identified because spectral GR logs were biased by the bituminous shales.

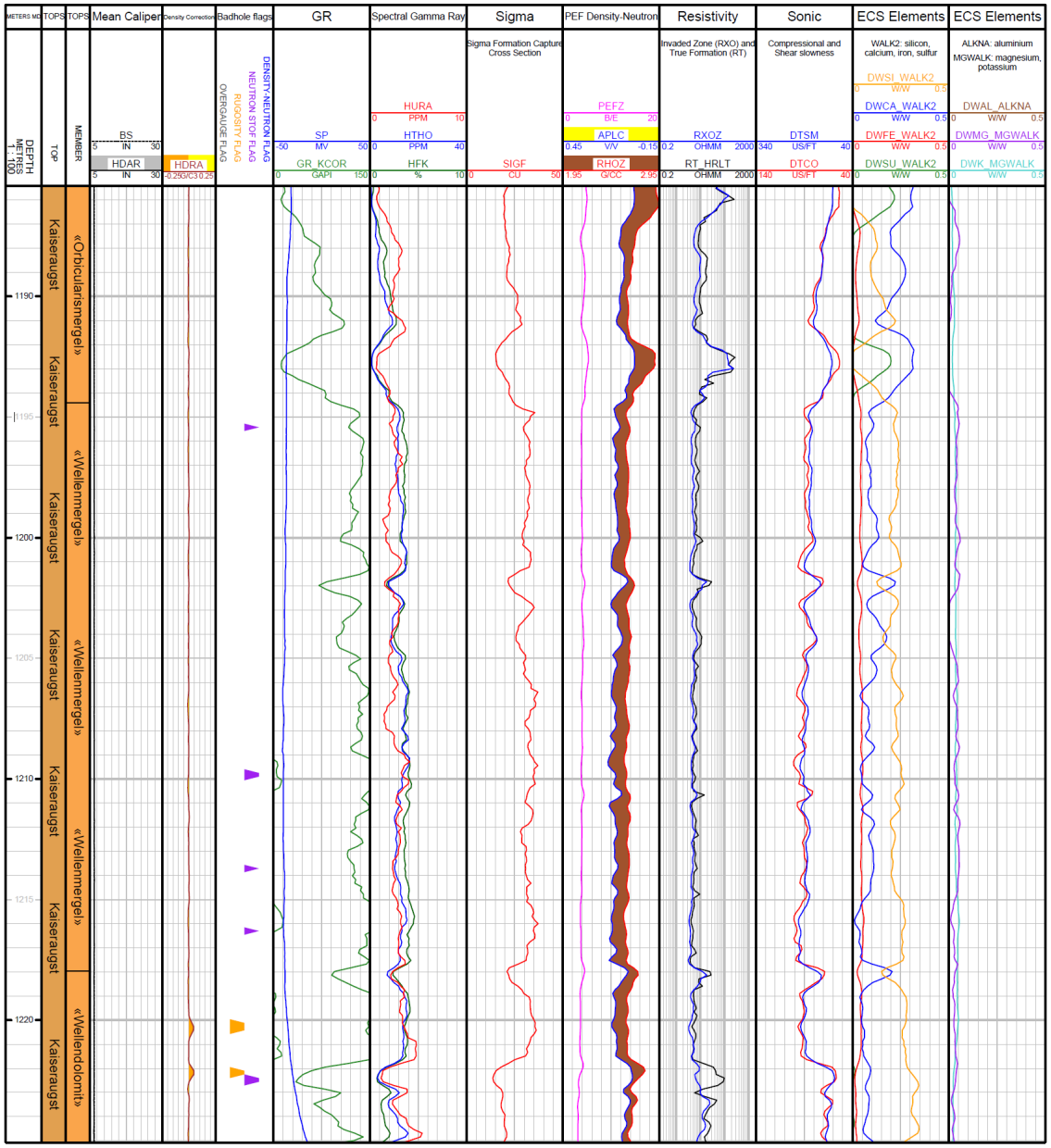


Fig. 3-9: Main logs of the composite dataset in the Kaiseraugst Formation

### 3.4.10 Dinkelberg Formation (1'225.07 m to 1'237.94 m MD)

The top of the Dinkelberg Formation corresponds to the transition from the heterogeneous carbonates, claystones and sandstones of the Kaiseraugst Formation to low-clay sandstones, which is represented in the logs by an increase in the silicon content (DWSI) and a decrease in calcium (DWCA), as well as with a very distinctive change in the density-neutron separation, where the density log shifts to the left of the neutron log ("crossover" in a limestone-compatible scale, shaded yellow).

Logs respond well to lithology in this formation because hole conditions were good (except in a short overgauge and rugose zone) and are characterised by the following attributes (Fig. 3-10):

- Logs often show a high total GR (GR_KCOR) ranging from 38 to 137 GAPI, despite the crossover in the density-neutron separation that is indicative of a low clay content and mineralogy dominated by siliciclastics. This is typical for siltstones and sandstones that contain slightly radioactive minerals such as K-feldspar and mica (and are better quantified by the stochastic, multimineral analysis described in Dossier X). The relatively high potassium concentrations (HFK), ranging from 0.47% to 2.9%, also suggest the presence of radioactive minerals.
- Photoelectric factor values (PEFZ) are close to that of pure quartz (1.8 B/E) in the Dinkelberg Formation, averaging at 2.3 B/E. The silicon content (DWSI) also suggests the presence of significant quartz, ranging from 0.26 to 0.47 W/W (pure quartz: 0.467 W/W).
- The separation between the shallow (RXOZ) and deep (RT_HRLT) resistivities indicates a permeable formation that has been invaded by the mud filtrate.
- The qualitative classification of clay minerals based on the spectral GR potassium (HFK) and thorium (HTHO) logs is not relevant given the low clay content.

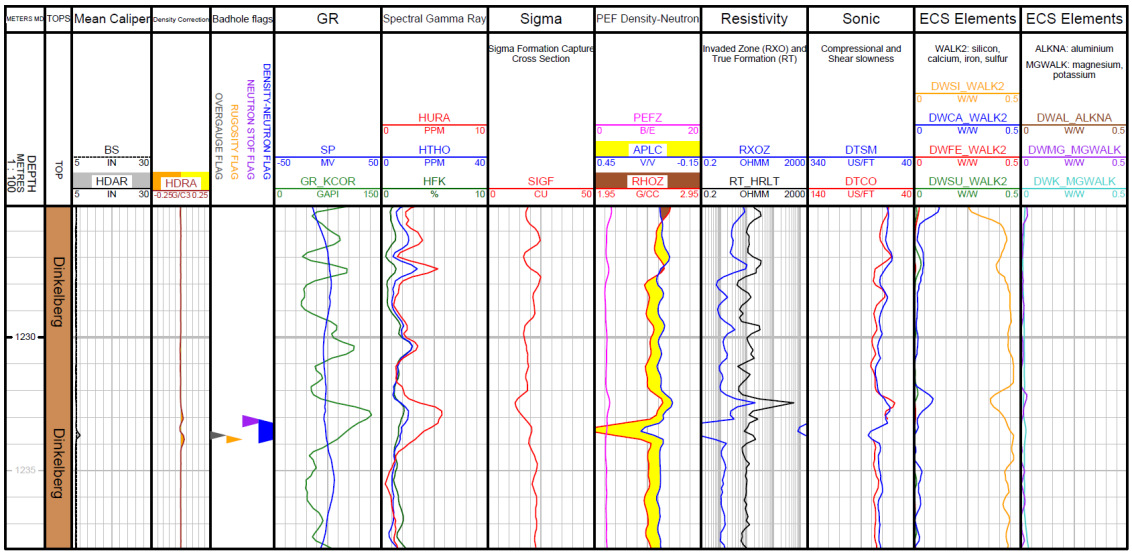


Fig. 3-10: Main logs of the composite dataset in the Dinkelberg Formation

### 3.4.11 Weitenau Formation (1'237.94 m to 1'288.87 m MD)

The top of the Weitenau Formation is characterised by sharp increases in the clay indicators such as total GR (GR_KCOR) and sigma (SIGF).

The base of the Weitenau Formation was not drilled.

Logs respond well to lithology in this formation because hole conditions were good (Fig. 3-11). Logs in the Weitenau Formation have the following attributes:

- A very high total GR, ranging from 82 to 232 GAPI, with a low density-neutron separation (displayed in the limestone-compatible scale), indicate relatively low clay contents. This is typical for siltstones and sandstones that contain slightly radioactive minerals such as K-feldspar and mica. The occurrence of arkose in this formation was reported by Blüm (1989), supporting this assumption.
- In a few zones, "crossover" is observed in the density-neutron separation (shaded yellow) indicating the presence of siliciclastic minerals such as quartz (and feldspars). This observation is supported by the high silicon content (DWSI: 0.25 to 0.44 W/W).
- Log characteristics are fairly homogeneous, which is best shown by the low variations in spectral GR contributions (potassium: HFK; thorium: HTHO; uranium: HURA).

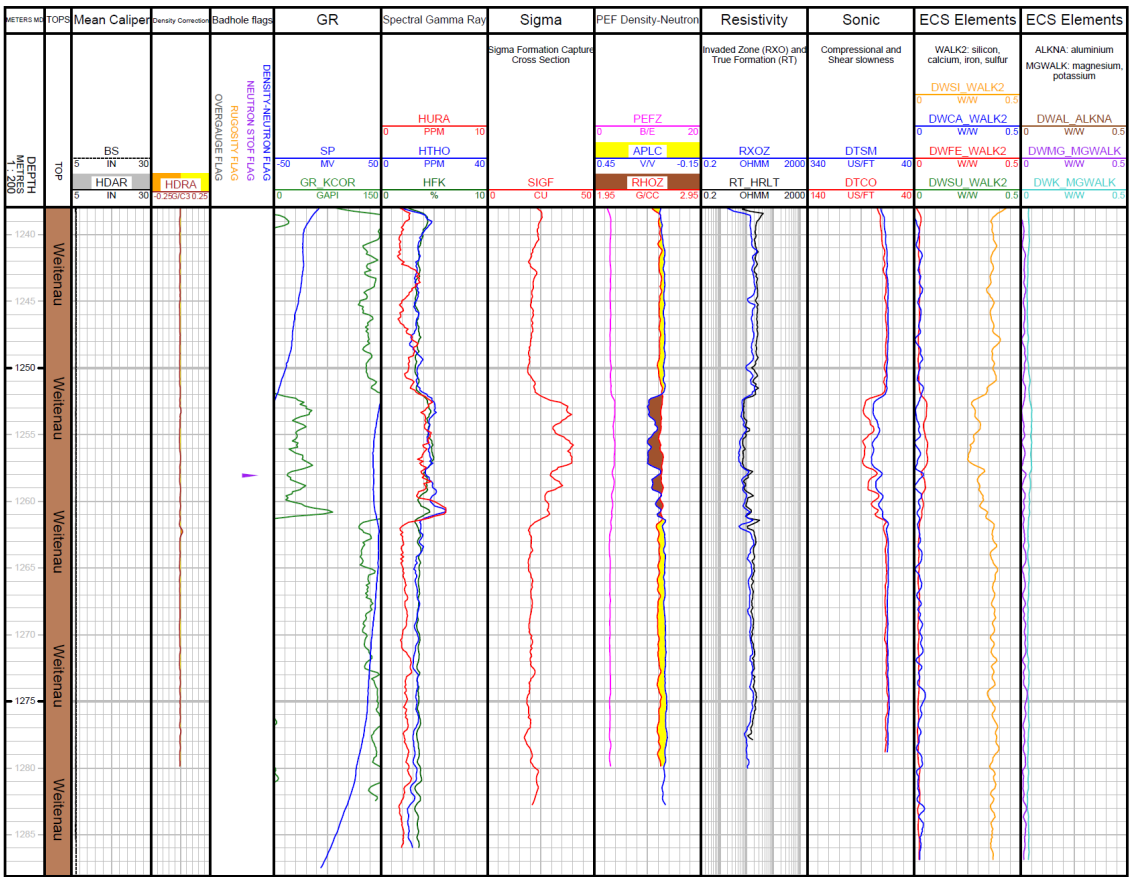


Fig. 3-11: Main logs of the composite dataset in the Weitenau Formation

## 3.5 Post-completion mud temperature

A temperature log was acquired by Schlumberger post-completion (in cased hole) on 04.07.2022 (Run 4.3.1) to measure the undisturbed temperature of the mud after the last mud circulation on 06.07.2021. Temperature was measured using the EMS tool, which has an accuracy of ± 1 °C and resolution of 0.1 °C. In Fig. 3-9, only the downlog from Run 4.3.1 is plotted as it is believed to be the most representative of the formation temperature. It was acquired at a slow rate of 175 m/hr to avoid mixing of the hydrostatic mud column. The fluid level during logging was at 53.8 m MD as shown by the change in temperature at this depth. The maximum temperature of 59.41 °C was recorded at 1'108.10 m (close to TD). In the Opalinus Clay, the temperature varies between 41.58 and 49.96 °C and the average geothermal gradient is $\Delta T/\Delta D = 0.079$ °C/m. The overall temperature gradient is higher in the clay-rich units of the Dogger compared to the calcareous units of the Malm and Muschelkalk.

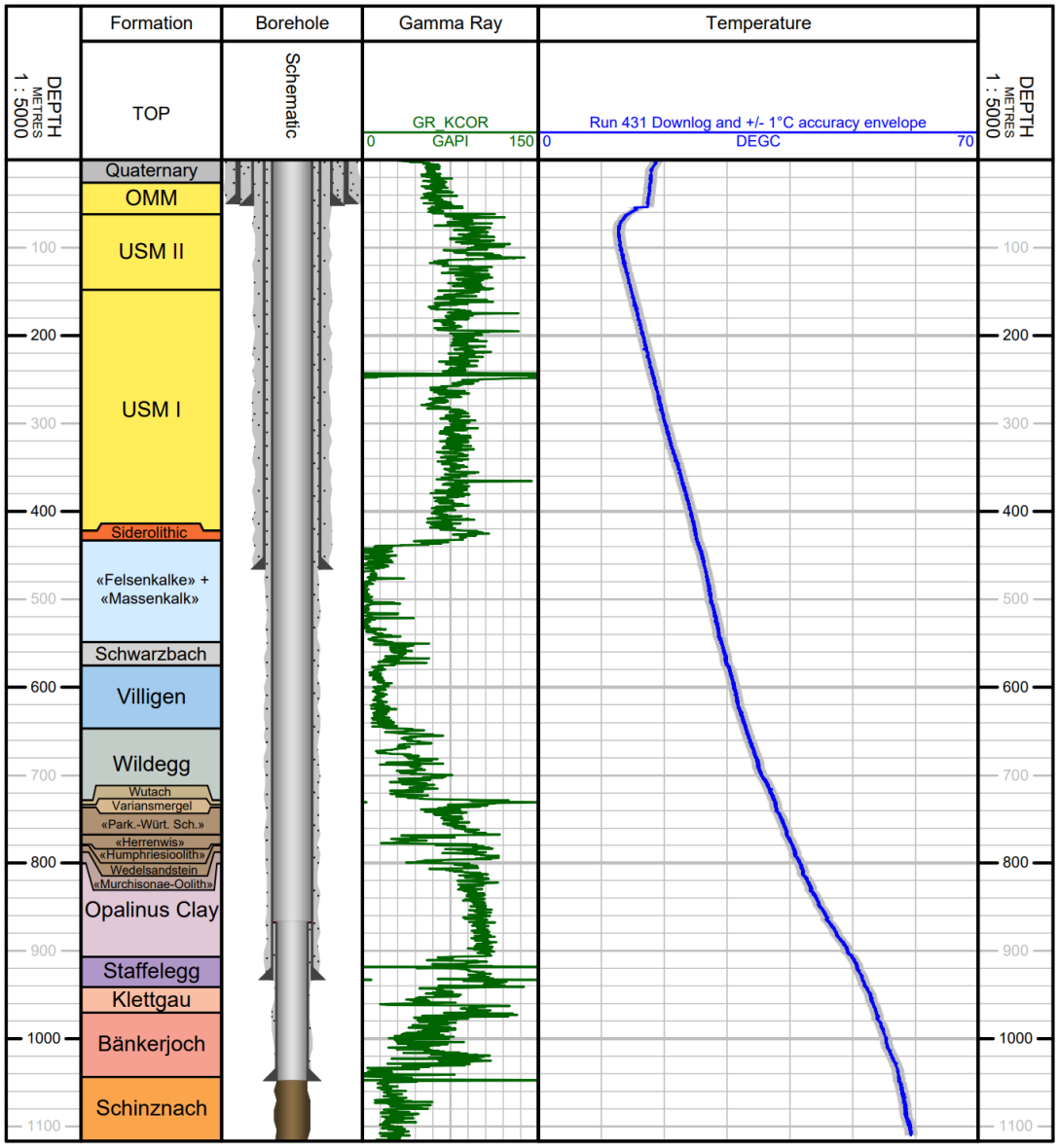


Fig. 3-9: Post-completion temperature log from the downlog pass of Run 4.3.1 (04.07.2022)

A ± 1 °C accuracy envelope is drawn in grey around the temperature log.

# 4 Borehole Imagery (BHI)

Borehole imaging tools produce high resolution circumferential images of the borehole wall by measuring either resistivity with tool pad contact or ultrasonic velocity. For the STA2-1 borehole, SLB's Fullbore Formation MicroImager (FMI) and Ultrasonic Borehole Imager (UBI) were used. The FMI comprises of four pads that measure the formation resistivity via an array of buttons (24 per pad) that are pressed against the borehole wall, providing a vertical resolution of 2.5 mm and 80% coverage in an 8" hole diameter. The UBI has a rotating sub that sends out acoustic pulses to the formation and measures the amplitude and travel time of the returning signals, providing 5 mm vertical resolution and 100% borehole coverage. In general, fractures, faults and bedding are more easily identifiable using the FMI than the UBI as the microresistivity images provide better contrast. However, borehole wall features can be missed if they are located in an area not covered by the tool pad, which is why FMI and UBI images should be used together for image interpretation. In addition, breakouts are typically poorly resolved on microresistivity images because fracturing and spalling associated with these breakouts result in poor contact of the tool pads with the borehole wall.

BHI was used to:

- identify and characterise geological, sedimentological and structural features including bedding, fault planes / zones and fractures
- identify stress-induced borehole phenomena such as tensile drilling-induced fractures and breakouts
- perform core goniometry
- select MHF and PMT testing locations (referred to as stations herein)
- detect and orient fractures induced by MHF stress measurements

For details on the first three uses of BHI, please refer to Dossier V. Only the latter two will be discussed further in the present Dossier.

The BHI, that was acquired pre-MHF, was quality-controlled (QCed), processed and interpreted by NiMBUC Geoscience in a limited amount of time (i.e. rush processing and basic quicklook interpretation). The aim of this quicklook interpretation was to provide a general and quick picture of existing borehole / rock heterogeneities (breakouts, natural and induced fractures etc.) for the selection of MHF and PMT stations immediately after BHI log acquisition and prior to MHF / PMT. In Fig. 4-1, the workflow used by NiMBUC Geoscience is described. Final processed and spliced pre-MHF image logs are included in Dossier V (Appendix B and Appendix C).

The post-MHF imagery underwent a similar workflow to the pre-MHF imagery, however, only the intervals that underwent stress testing were interpreted. These will be detailed in a future MHF interpretation report. To determine whether fractures were generated or enhanced (opened further), the pre- and post-MHF imagery was plotted side-by-side, along with the MHF test interval, packer positions and core photographs (see Appendix D).

| **Step 1: Image QC** | |
|---|---|
| Depth matching | Correlate high resolution image with reference GR |
| Caliper check | Verify calibration with casing ID, identify if borehole conditions could affect image quality (washouts, mud cake etc.) |
| Hardware check | Identify if downhole equipment performance indicators such as gain and voltage supply are consistent |
| Orientation check | Ensure orientation data are in agreement with borehole azimuth and deviation from independent survey |
| Accelerometer check | Accelerometer measurement should be consistent with earth's gravity (1 g = 9.81 ± 0.03 m/s$^2$) |
| Magnetometer check | Magnetometer consistent with theoretical magnetic field strength at location, X-Y magnetometers behave complementary, QC magnetic declination parameters input |
| Tool movement check | Identification of any stick and pull events using tension and accelerometer measurements |
| Acquisition check | Verify frame time and cable speed control |
| Borehole image check | Identification of dead buttons or pads and any casing interference |

| **Step 2: Image processing** | |
|---|---|
| Basic image generation | Azimuthal orientation of images to true or grid north |
| | Merging of individual tool run passes |
| | Splicing of data between drilling sections |
| | If required, invert images to ensure per industry standards that low value = low resistivity and high value = high resistivity |
| | If required, correct offsets between pad images |
| | Bad button detection and correction |
| Image equalisation and normalisation | Static normalisation involving selecting the normalisation distribution (uniform/Gaussian), equalisation strength, high/low cut-offs for equalisation etc. |
| | Dynamic normalisation to enhance local contrasts highlighting features in a selected sliding window of a few metres |

| **Step 3: Basic interpretation** | |
|---|---|
| Manual picking of features directly from the processed image in accordance with Nagra classification scheme detailed here | Drilling-induced fractures |
| | Borehole breakouts |
| | Bedding |
| | Fractures (conductive, partially conductive, resistive, partially resistive, faint trace) |
| | Faults (conductive, partially conductive, resistive, partially resistive, faint) |

Fig. 4-1: Borehole image processing workflow

# 5 Micro-hydraulic Fracturing (MHF)

## 5.1 Introduction and objectives

A series of stress measurements were performed in the STA2-1 borehole using the Micro-hydraulic Fracturing (MHF) technique. MHF testing in boreholes is the only direct method available for measuring rock stress magnitude at great depth. An overview of the methodology can be found in Haimson (1993), Desroches & Kurkjian (1999) and Haimson & Cornet (2003) and references therein. Recent updates on the methodology, some of which having been specifically designed for this project, can be found in Desroches et al. (2021a, 2021b).

The objectives of the testing programme are to acquire data to:

- provide estimates of the in situ stress state in the Opalinus Clay and adjacent rock formations, and
- provide calibration points for mechanical earth models (MEM) of the rock mass (1D, 3D). See Bérard & Prioul (2016) for an overview of mechanical earth models and Plumb et al. (2000) for a definition of an MEM.

Key features include:

- Core images and BHI (FMI and UBI) were used to select the appropriate test depths closest to where geomechanical lab test samples were taken.
- The MHF protocol that was used, was tailored in real-time to bracket the far-field closure stress as closely as possible.
- Post-MHF imaging logs were run to determine the trace of the newly created fractures, enabling better allocation of the MHF closure stress to a principal stress direction.
- Sleeve fracturing was regularly used to focus the test on the desired interval; sleeve reopening was used to allow the estimation of the maximum horizontal stress when the MHF tests yielded an estimate of the minimum horizontal stress.

## 5.2 MHF theory

MHF tests an interval of approximately 1 m which is sealed above and below by packers that are approximately 0.5 m in length (exact dimensions are dependent on the configuration of the tool string). A schematic, showing the first two hydraulic fracturing cycles for a typical MHF test, is presented in Fig. 5-1. Once the interval is sealed, a micro-hydraulic fracturing cycle begins with pressurising the interval (1$^{st}$ step) until fracture initiation. Fluid keeps being injected to extend the micro-hydraulic fracture into the formation by a couple of decimetres (2$^{nd}$ step). Injection is then stopped to allow fracture closure, and pressure fall-off is observed (3$^{rd}$ step). Similar steps are repeated to further extend and refine the testing of the micro-hydraulic fracture until the test is deemed satisfactory. Tests performed in this borehole have included more complex testing techniques as reported in Desroches et al. (2021a).

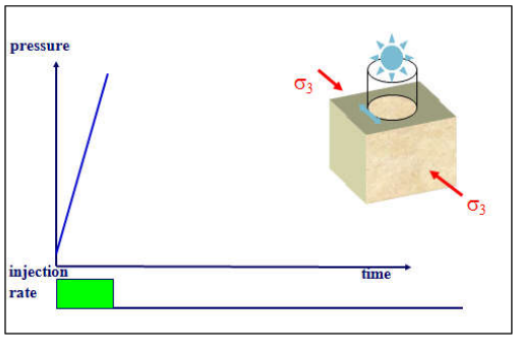


1st step: pressurisation

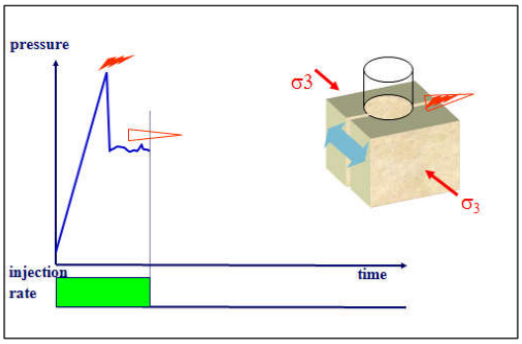


2nd step: fracture propagation

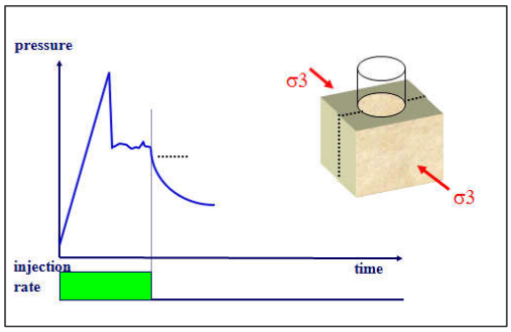


3rd step: Fracture closure

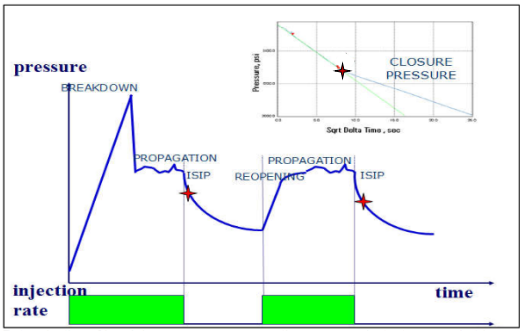


Repeat steps for subsequent cycle(s)

Fig. 5-1: Schematic showing the response of the interval pressure to fluid injection in the interval as a function of time during an MHF test and associated formation response (courtesy of SLB)

## 5.3 Test protocol

Each test consisted of a succession of steps according to the general test procedure described in Desroches & Kurkjian (1999), Haimson & Cornet (2003) and Wileveau et al. (2007). Although a general procedure was followed for each test, the steps were tailored in real-time to ensure that the pressure records provided the best possible estimate for closure stress (see Desroches et al. 2021b). As a result, the number of steps and their nature varied from test to test.

The steps undertaken during a stress test were as follows:

- Depth correlation: validate the cable depth by comparing GR log with the reference GR log of the borehole.
- Sleeve fracturing: this step is analogous to sleeve reopening (see below) but performed prior to the micro-hydraulic fracturing operation. The single packer is placed in front of the desired depth and applies pressure to focus the initiation of a longitudinal fracture at the desired interval. Note that this part of the sequence is not carried out if a pre-existing fracture (natural or drilling-induced or -enhanced) is present in the test interval.
- Packer inflation and leak-off test: the straddle packer is positioned so that the centre of the interval is in front of the desired depth. Packers are inflated to a differential pressure of 300 to 500 psi and the integrity of the seal is observed. The integrity of the seal is further validated by a short injection into the interval.

- Breakdown cycle (steps 1 to 3 in Fig. 5-1): the first cycle in a test during which a hydraulic fracture is propagated was counted as a breakdown cycle (even if technically there is no breakdown, e.g. because a pre-existing drilling-induced fracture was tested). To ensure that cycles are not counted more than once, there was only one breakdown cycle per test. Whether it starts with a step-rate test or ends with a slamback / rebound test (see below), it is still only counted as one breakdown cycle.
- Reopening cycle: any subsequent injection / shut-in cycle during which a fracture is propagated and that neither starts with a step-rate test nor ends with a slamback / rebound test (see below) is counted as a reopening cycle.
- Slamback / rebound test: at the end of an injection cycle during which a fracture was propagated (but not for the first time), the interval is quickly opened and closed for a fast depressurisation, and pressure rebounds from a value close to borehole hydrostatic pressure. The slamback occurs immediately after the injection stopped, and the rebound is observed until a plateau is reached. If the injection cycle starts with a step-rate test, it is only counted as a step-rate test and not as a slamback / rebound test.
- A new procedure ('forced closure') was introduced in the BOZ1-1 borehole and retained for subsequent boreholes. Because it also involves withdrawing fluid from the interval, cycles with forced closure were not counted separately but were also counted as S/R tests.
- Step-rate test: an injection cycle during which the rate was increased (or decreased) in steps with at least three different flow rates during the cycle is called a step-rate test. An injection cycle during which the rate was only changed once cannot be counted as a step-rate test because it does not allow a step-rate interpretation.
- Sleeve reopening: the single packer is moved in front of the previously tested interval and pressure is applied with the aim of detecting and reopening the fracture created during the micro-hydraulic fracturing cycles.

In Fig. 5-2, an example of the pressure record for a MHF test performed in the STA2-1 borehole is presented (Station 3-1, Run 2.4.3). Fig. 5-2a shows the pressure in the interval (PAQP) and the inflate pressure of the packers (PAHP), Fig. 5-2b the fluid injection rate as a function of time (pump speed is in blue, pump piston direction in yellow/colourless), Fig. 5-2c the injected volume as a function of time (POTCV) as well as the position of the valve controlling the packers (PAFP, 0-closed, 128-open) and Fig. 5-2d, also called a reconciliation plot, displays the characteristic pressures estimated for all cycles for which a fracture was created / tested. For this test, there were a total of 4 MHF cycles, labelled 5 to 8. The first cycles are not analysed as they correspond to the packer inflation and leak-off test. Fracture initiation ("breakdown") took place during cycle 5, which corresponds to the breakdown / propagation cycle depicted in the theory schematic (Fig. 5-1). Cycles 6 and 8 are reopening tests, cycle 7 is a step-rate test. A slamback / rebound test was performed at the end of cycle 7, and a forced closure procedure was performed at the end of cycle 6. The characteristic pressures presented in Fig. 5-2d reflect the stress acting on the fracture: they validate the creation of a hydraulic fracture and exhibit a rather constant behaviour, which supports that an estimate of the far-field stress can be obtained from the test.

The raw MHF pressure-time and reconciliation plots for all tests conducted in the STA2-1 borehole are included in Appendix E. In Tab. 5-1, a summary of the steps taken for each MHF station is given, along with the associated formation / unit that was tested. Stations are presented in operational order of the first attempt for each station.

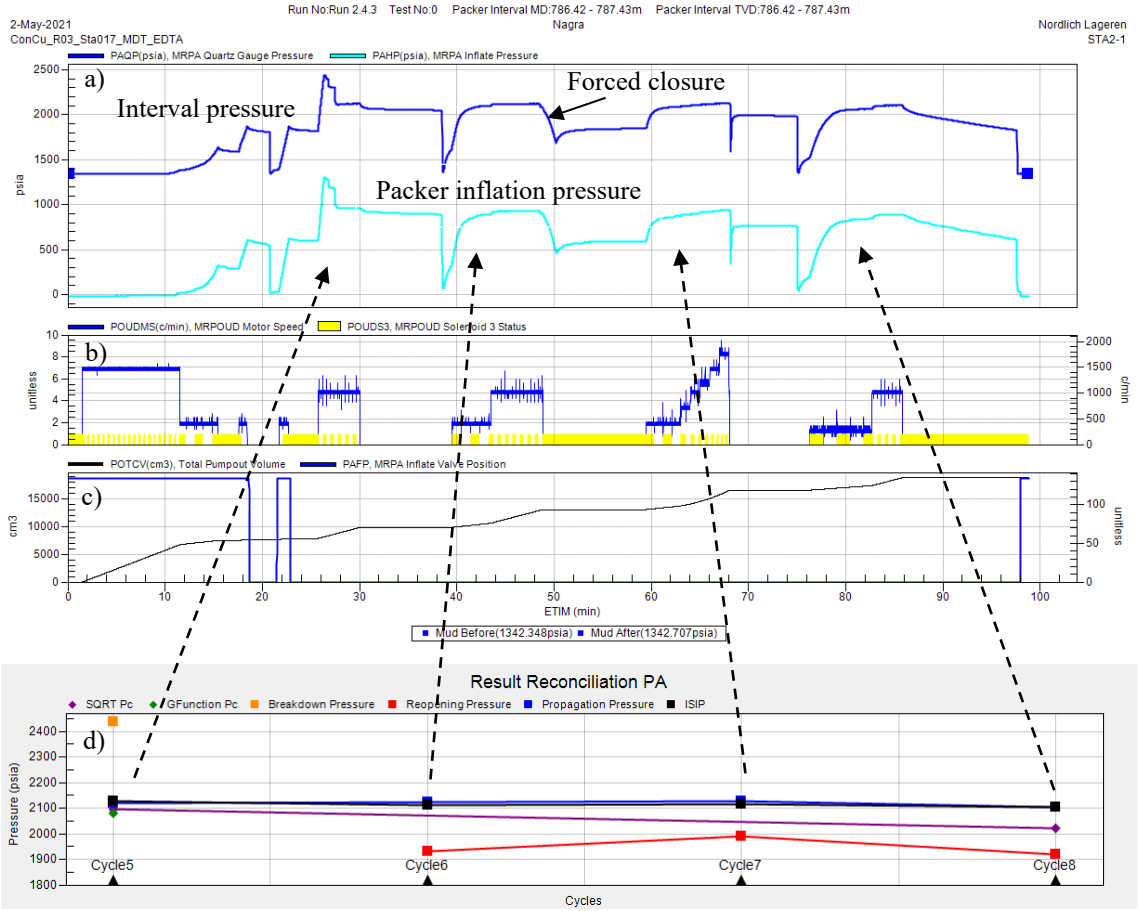


Fig. 5-2: Example of pressure record for MHF test from STA2-1 (Station 3-1, Run 2.4.3)
Pc stands for closure pressure.

Tab. 5-1: Summary of MHF station locations and operations carried out for each section of the STA2-1 borehole

| Phase / Section | Station | Formation / unit | Middle interval depth [m] | Sleeve fracturing cycles | Break-down cycles | Re-opening cycles | Slamback / rebound tests | Step-rate tests | Sleeve reopening cycles |
|---|---|---|---|---|---|---|---|---|---|
| II (Run 2.4.3) | 1-1 | Opalinus Clay | 897.40 | 2 | 1 | 2 | 1 | 1 | 2 |
| | 5-1 | «Felsenkalke» + «Massenkalk» | 543.90 | 2 | 1 | 1 | 1 | 1 | - |
| | 5-1a | | | - | 1 | 1 | 1 | 1 | 2 |
| | 2-1 | Staffelegg Fm. | 909.00 | 2 | 1 | 2 | 1 | 2 | 2 |
| | 3-1 | «Murchisonae-Oolith Fm.» | 787.05 | 2 | 1 | 1 | 1 | 1 | 2 |
| | 1-3 | Opalinus Clay | 812.25 | 2 | 1 | 3 | 1 | 2 | 2 |
| | 4-1 | «Parkinsoni-Württembergica-Sch.» | 749.50 | 2 | 1 | 2 | 3 | 2 | 3 |
| | 6-1 | Wildegg Fm. | 678.15 | 2 | 1 | 2 | 1 | 2 | 2 |
| | 1-2 | Opalinus Clay | 830.30 | 2 | 1 | 0 | 2 | 2 | 2 |
| | 7-1 | Schwarzbach Fm. | 562.85 | 2 | 1 | 0 | 1 | 1 | 0 [a] |
| III (Runs 3.2.3 & 3.2.4) | 1-1 | Klettgau Fm. | 940.75 | 2 | 1 | 0 | 1 | 1 | - |
| | 1-1b | | | - | - | 2 | - | 2 | 2 |
| | 2-1 | Klettgau Fm. | 966.65 | 2 | 1 | 1 | 1 | 2 | 0 [b] |
| | 2-2 | Klettgau Fm. | 953.25 | 2 | 1 | 3 | 1 | 3 | 3 |
| | 3-2 | Bänkerjoch Fm. | 1'037.30 | 2 | - | - | - | - | - |
| | 3-1 | Bänkerjoch Fm. | 983.10 | 2 | - | - | - | - | - |
| | 3-1b | | | - | 1 | 2 | 2 | 2 | 2 |
| | 3-3 | Bänkerjoch Fm. | 1'010.20 | 2 | 1 | 4 | 3 | 3 | 2 |
| IV (Runs 4.1.9 & 4.2.3) | 1-1 | Weitenau Fm. | 1'280.70 | 0 | 1 | 4 | 0 | 2 | 0 [c] |
| | 1-2 | Weitenau Fm. | 1'259.30 | 2 | 1 | 2 | 1 | 2 | 0 [d] |
| | 4-1 | Schinznach Fm. | 1'055.25 | 2 | 1 | - | - | - | - |
| | 4-3 | Schinznach Fm. | 1'079.00 | 2 | 1 | 3 | 0 | 2 | 2 |
| | 3-1 | Zeglingen Fm. | 1'128.90 | 3 | 1 | 1 | 2 | 2 | 2 |
| | 4-2 | Schinznach Fm. | 1'074.35 | 0 | 1 | - | - | - | - |
| | 4-2a | | | | - | 2 | 0 | 3 | 2 |
| | 3-2 | Zeglingen Fm. | 1'131.95 | 2 | 1 | 2 | 1 | 2 | 2 |

[a] Sleeve reopening was not performed as time was insufficient at the end of the testing campaign

[b] Sleeve reopening was not performed as the MHF test was unsuccessful

[c] Sleeve reopening was not performed as the rathole length was insufficient

[d] Sleeve reopening was not performed as the tool was fished after the MHF test

## 5.4 MHF results

22 tests were attempted (some in two stages), with 19 of them being successful, from the «Felsenkalke» + «Massenkalk» (433 m) down to the Weitenau Formation (1288.12 m). Tests without the ability to breakdown the formation or with an inability to maintain a high-pressure seal were deemed unsuccessful. Any other test where a closure stress could be estimated was deemed successful.

Tab. 5-2 presents a quicklook interpretation of the MHF results which includes the 'breakdown pressure', the closure stress range and associated comments. The 'breakdown pressure' is taken as the maximum pressure reached during the first hydraulic fracturing cycle. If no fracture was propagated, that value is still reported but followed by an asterisk. A classical breakdown pressure interpretation should not be applied to these pressure values because sleeve fracturing was performed prior to hydraulic fracturing. Recorded 'breakdown pressures' are therefore technically reopening pressures. The closure stress acts normal to the fracture surface. Its range was determined from the pressure records and expressed with a lower and an upper bound.

Fig. 5-3 plots the closure stress ranges from the quicklook analysis as a function of depth together with the overburden vertical stress (Sv), estimated from integration of the density logs over depth, and the maximum pressures measured during the formation integrity tests (FIT).

Tab. 5-2: Quicklook interpretation of MHF results for STA2-1 borehole

| **Section Run Diameter** | **Station** | **Formation** | **Depth** [m] | **Breakdown pressure** [MPa] | **Closure stress range** [MPa] | **Comments** |
|---|---|---|---|---|---|---|
| II Run 2.4.3 8½" bit size | 5-1 | «Felsenkalke» + «Massenkalk» | 543.90 | 22.26 | 14.48 – 17.79 | $S_{hmin}$ likely |
| | 7-1 | Schwarzbach Fm. | 562.85 | 33.31 | 10.90 – 18.62 | High propagation / closure pressure >> $S_v$; upper bound $S_{hmin}$ |
| | 6-1 | Wildegg Fm. | 678.15 | 23.80 | 12.28 – 14.83 | Multiple closures; $S_{hmin}$ likely |
| | 4-1 | «Parkinsoni-Württembergica-Sch.» | 749.50 | 18.49 | 12.59 – 14.83 | Multiple closures; $S_{hmin}$ likely |
| | 3-1 | Wedelsandstein | 787.05 | 16.82 | 13.23 – 14.48 | $S_{hmin}$ likely |
| | 1-3 | Opalinus Clay | 812.25 | 17.38 | 13.93 – 15.55 | $S_{hmin}$ likely |
| | 1-2 | Opalinus Clay | 830.30 | 18.55 | 13.10 – 15.17 | $S_{hmin}$ likely |
| | 1-1 | Opalinus Clay | 897.40 | 21.28 | 15.66 – 17.41 | $S_{hmin}$ likely |
| | 2-1 | Staffelegg Fm. | 909.00 | 21.68 | 15.03 – 18.79 | $S_{hmin}$ likely |
| III Runs 3.2.3 & 3.2.4 8½" bit size | 1-1 | Staffelegg Fm. | 940.75 | 19.38 | 17.24 – 18.79 | $S_{hmin}$ likely |
| | 2-2 | Klettgau Fm. | 953.25 | 38.28 | 14.59 – 23.10 | Fracture sensed both $S_{hmin}$ and $S_v$; propagation pressure significantly larger than $S_{hmin}$ |
| | 2-1 | Klettgau Fm. | 966.65 | 19.18* | n/a | Short fracture under one of the packers likely |
| | 3-1 | Bänkerjoch Fm. | 983.10 | 23.42 | 16.34 – 19.14 | Multiple closures; $S_{hmin}$ likely |
| | 3-3 | Bänkerjoch Fm. | 1'010.20 | 35.09 | 18.97 – 25.79 | Multiple closures; $S_{hmin}$ likely |
| | 3-2 | Bänkerjoch Fm. | 1'037.30 | 43.45* | n/a | Breakdown attempted for more than 3 h; packer bypass developed before breakdown in interval |
| IV Runs 4.1.9 & 4.2.3 6⅜" bit size | 4-1 | Schinznach Fm. | 1'055.25 | 16.54* | n/a | Could not maintain packer seal |
| | 4-2 | Schinznach Fm. | 1'074.35 | 26.55 | 14.48 – 17.03 | High leak-off; $S_{hmin}$ likely |
| | 4-3 | Schinznach Fm. | 1'079.00 | 26.14 | 17.00 – 19.76 | $S_{hmin}$ likely |
| | 3-1 | Zeglingen Fm. | 1'128.90 | 28.64 | 21.38 – 24.14 | Slanted fracture at the borehole wall, therefore wide range of $S_{hmin}$ |
| | 3-2 | Zeglingen Fm. | 1'131.95 | 25.78 | 20.07 – 23.79 | $S_{hmin}$ likely |
| | 1-2 | Weitenau Fm. | 1'259.30 | 24.21 | 21.24 – 22.55 | $S_{hmin}$ likely |
| | 1-1 | Weitenau Fm. | 1'280.70 | 25.08 | 19.38 – 20.83 | $S_{hmin}$ likely |
| Total number of tests | | | | | | 22 |
| Total number of successful tests | | | | | | 19 |
| Success rate (actual vs. attempted) & (actual vs. desired from initial plan) | | | | | | 86% & 106% |

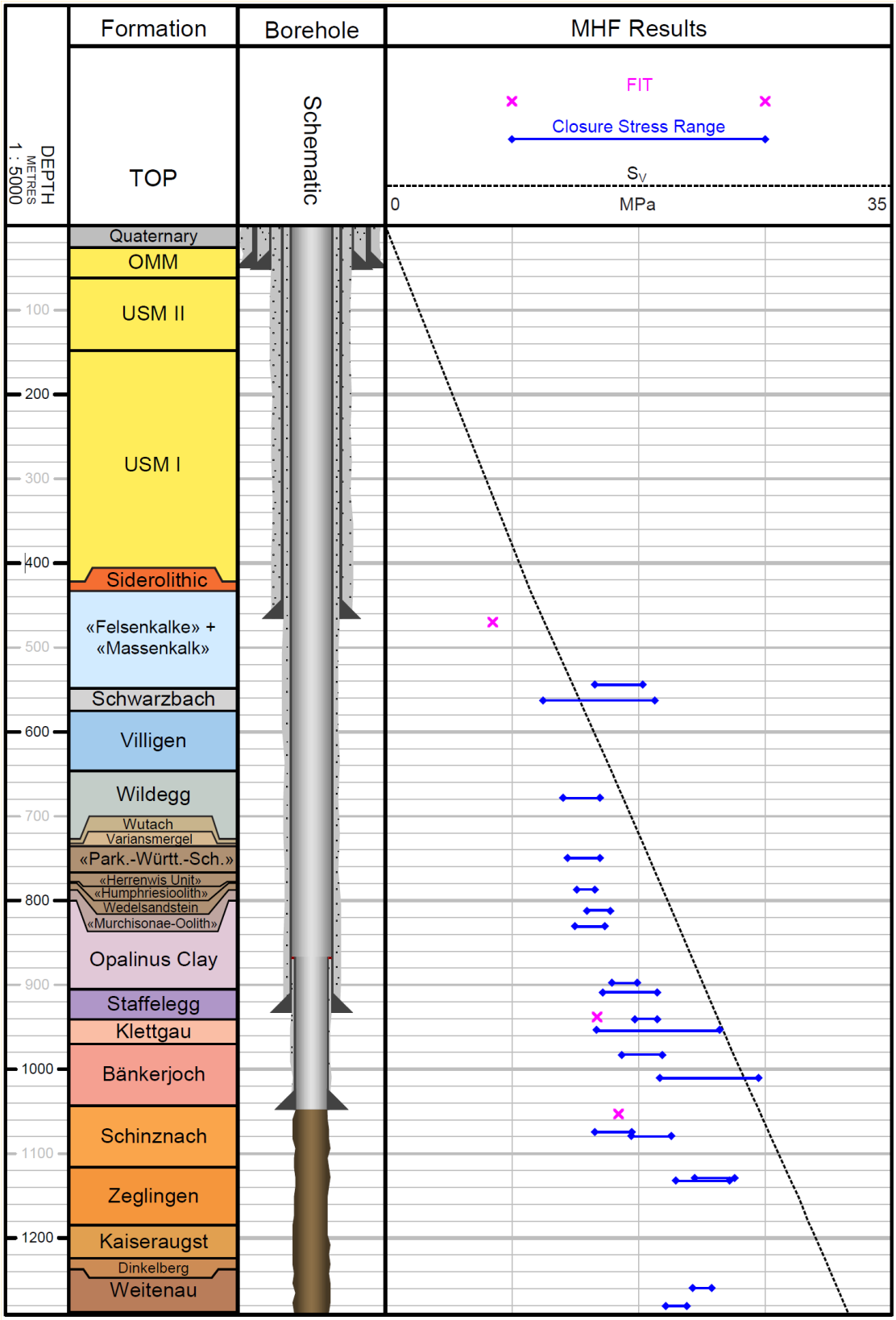


Fig. 5-3: Comparison of the quicklook closure stress range obtained from the STA2-1 MHF tests with the overburden vertical stress (Sv) from the integration of density over depth and the maximum pressures attained during the formation integrity tests (FIT)

Quicklook analysis of the post-MHF borehole imagery showed that new or enhanced features (longitudinal) could be observed at successful station locations. Conversely, in unsuccessful tests, no new feature could be observed. Fig. 5-4 presents the pre- and post-MHF images for Station 1-1 (Run 3.2.3). Note that there were no pre-existing fractures on the pre-MHF images. New fracture segments induced by the MHF test can be seen on the dynamic post-FMI image and are highlighted by black boxes on the rightmost track. The MHF test led to the creation of vertical conductive fractures at the wellbore. The azimuth of these new fracture traces indicates the azimuth of the maximum horizontal stress. A comparison of all the pre- and post-MHF borehole images is included in Appendix D.

Interpretation of sleeve fracturing / sleeve reopening tests was not performed as part of the acquisition programme and is not included in this report.

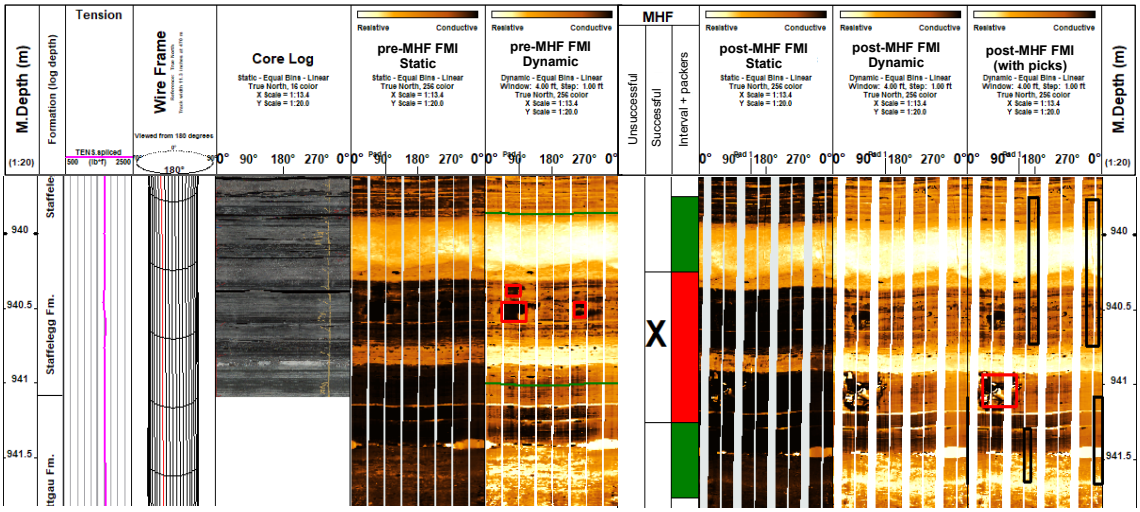


Fig. 5-4: Example of pre- vs. post-MHF images from STA2-1 (Station 1-1 from Run 3.2.3, Section III)

Pre- and post-MHF images are presented on the left and right of the MHF columns, respectively.

New fracture traces created by the MHF test are shown by black boxes picked by NiMBUC Geoscience on the post-FMI dynamic image.

# 6 Pressure-meter Testing (PMT)

## 6.1 Introduction and objectives

PMT tests were conducted to estimate the in situ shear modulus by testing a larger volume of rock than is possible during laboratory tests of core samples and at larger strains than during sonic logging. Testing was performed during MHF operations using the single packer module that is used to perform sleeve fracturing and sleeve reopening as discussed in Chapter 5. The main objective of the PMT programme in the STA2-1 borehole was to obtain an interpretable pressure record in the Opalinus Clay, which could then be compared with the dilatometer tests planned in the STA3-1, STA2-1 and BAC1-1 boreholes. A calibration point was also required for PMT interpretation, which can be performed in either a casing joint, a formation of known stiffness or a formation that is stiffer than the tool.

PMT previously undertaken in the BOZ1-1 and BOZ2-1 boreholes explored different tool string combinations and protocols to find the best possible hardware / methodology for obtaining an interpretable pressure record in the formation of interest. Based on experience from these tests, PMT at STA2-1 was undertaken using the reduced protocol, a faster methodology developed to perform a test faster prior to sleeve fracturing, and the Frac12k packer deployed with the auto retract mechanism (ARM) coupled to a constant flow rate pump.

## 6.2 Test protocol

A series of cycles with increasing maximum pressure were conducted to avoid creating a tensile fracture during the first cycle.

All tests were initiated with a packer inflation procedure, the aim of which was to ease the packer into place at the station location.

After packer inflation was complete, a series of inflation / deflation cycles were undertaken using the reduced protocol that was developed during the BOZ1-1 PMT testing programme as a means of performing faster tests that could be done directly prior to the MHF sleeve fracturing test. This is in line with what is presented in the ASTM Standard D8359-20 (2020), "Standard test method for determining in situ rock deformation modulus and other associated rock properties using a flexible volumetric dilatometer".

Note that in the text below "pressure" refers to the packer inflation pressure. The packer inflation pressure is the differential pressure between the hydrostatic pressure in the borehole and the absolute fluid pressure in the packer: it is the pressure difference seen by the packer membrane. Describing the protocol in terms of a inflation pressure enables the same protocol to be used between stations (regardless of local station conditions which change with depth and formation).

*Packer inflation:*

- The packer is first inflated to a pressure of 250 psi; fall-off is observed for 5 min. The packer is then de-pressurised.
- The packer is re-inflated again to a pressure of 250 psi; fall-off is observed for 5 min. The packer is not de-pressurised before the next steps.

*Reduced protocol:*

- The packer is inflated to increasing pressure levels, in steps of 500 psi (e.g. 1'000 psi, 1'500 psi, 2'000 psi).
- For each inflation cycle, the packer is inflated at a constant flow rate to the desired level; fall-off is observed for 3 min.
- The packer is then deflated down to a pressure level of 30 psi to 50 psi to ensure that full contact between the packer and the borehole is maintained.
- The packer is then inflated to the next desired pressure level; fall-off is observed for 3 min followed by partial deflation, until the final desired pressure is reached. The final desired pressure should be below the formation breakdown pressure and is estimated from results of previous MHF tests in a similar formation.

## 6.3 Results

Two PMT tests were carried out using the Frac12k packer and MRPO module fitted with an extra-high-pressure displacement unit (XPDU) and a constant displacement pump. The first PMT was performed successfully in the Opalinus Clay, followed directly after by a calibration test in the stiff «Felsenkalke» + «Massenkalk» unit. Details of the PMT related operations are given in Tab. 6-1.

Due to a tool malfunction (damage observed on rubber membrane and coiled tubing), no dilatometer test results could be acquired for comparison with the PMT tests. Results can be compared with the sonic log and laboratory tests on core samples.

Tab. 6-1: PMT details

| **Section Run Diameter** | **Formation** | **Middle packer depth** [m] | **Protocol** |
|---|---|---|---|
| II<br>Run 2.4.3<br>8½" bit size | Opalinus Clay | 904.50<br>(performed directly before PMT #2) | Packer inflation protocol, followed by three cycles up to an inflation (differential) pressure of 1'000 psi, 1'500 psi and 2'000 psi, respectively. The hydrostatic pressure in the borehole (the reference pressure for the packer differential pressure) was measured to be 1'487 psi. |
| | «Felsenkalke» + «Massenkalk» | 543.75<br>(performed directly after PMT #1 and prior to SF at Station 5-1) | Packer inflation protocol, followed by three cycles up to an inflation (differential) pressure of 1'000 psi, 1'500 psi and 2'000 psi, respectively. The test ended with a repeat cycle up to 2'000 psi inflation pressure. The hydrostatic pressure in the borehole (the reference pressure for the packer differential pressure) was measured to be 856 psi. |

The raw PMT time plots for all tests conducted in the STA2-1 borehole are included in Appendix F. The pressure record of the PMT conducted in the «Felsenkalke» + «Massenkalke» is presented in Fig. 6-1. First the packers were inflated to a low inflation pressure twice to ease their position against the borehole wall as per inflation protocol described earlier. Three inflation cycles were then performed up to pressures of 1'500 psi (with a stop at 1'000 psi), 2'000 psi and 2'000 psi, respectively, with near full packer depressurisation in between. These three cycles were then followed by regular sleeve fracturing (SF) cycles without moving the tool.

An example of a possible interpretation methodology is presented in ASTM D8359-20 (2020). Interpretation of the PMT is being performed separately by Schlumberger as part of a special project with Nagra and further results are therefore not reported here. In particular, refinement of results in consideration of the calibration tests is still under investigation.

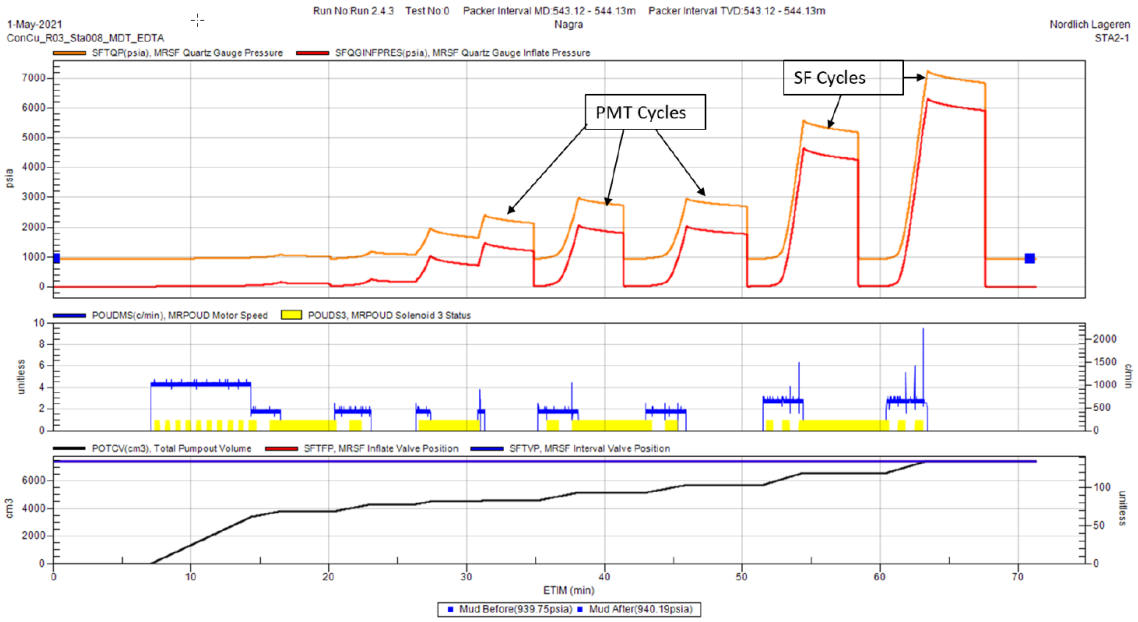


Fig. 6-1: Time summary plot for PMT operation carried out before the SF for MHF Station 5-1 (Run 2.4.3)

Top plot: packer inflation pressure (red) and packer absolute pressure (orange) – the difference between the two is the borehole hydrostatic pressure; middle plot: pump speed (blue) and piston direction (yellow / colourless); bottom plot: total injected volume (black).

# 7 References

ASTM D8359-20 (2020): Standard Test Method for Determining the In Situ Rock Deformation Modulus and Other Associated Rock Properties Using a Flexible Volumetric Dilatometer. DOT:10.1520/D8359-20.

Bérard, T. & Prioul, R. (2016): Mechanical Earth Model. Oilfield Review: The Defining Series, https://www.slb.com/resource-library/oilfield-review/defining-series/defining-mem.

Blüm, (1989): Faciesanalyse im Rotliegenden des Nordschweizer Permokarbon-Trogs (Hochrhein-Region zwischen Basel und Laufenburg). Eclogae geol. Helv., 82(2), 455-489.

Desroches, J. & Kurkjian, A.L. (1999): Applications of wireline stress measurements. Paper SPE-58086, SPE Reservoir Evaluation & Engineering 2/5, 451-461. DOI:10.2118/ 58086-PA.

Desroches, J., Peyret, E., Gisolf, A. Wilcox, A., Di Giovanni, M., Schram de Jong, A., Sepehri, S., Garrard, R. & Giger, S. (2021a): Stress measurement campaign in scientific deep boreholes: Focus on tool and methods. SPWLA Paper #2021-056 presented at the SPWLA 62nd Annual Logging Symposium, May 17-20 2021.

Desroches, J., Peyret, E., Gisolf, A., Wilcox, A., di Giovanni, M., Schram de Jong, A., Milos, B., Gonus, J., Bailey, E., Sepehri, S., Garitte, B., Garrard, R. & Giger, S. (2021b): Stress-Measurement Campaign in Scientific Deep Boreholes: From Planning to Interpretation. ARMA-2-21-1928 presented at the 55th U.S. Rock Mechanics/Geomechanics Symposium, Virtual, June 2021.

Haimson, B.C. (1993): The Hydraulic Fracturing Method of Stress Measurement: Theory and Practice. Chapter 14 in: Hudson, J. (ed.): Comprehensive Rock Engineering 3, 395-412, Pergamon Press. DOI: 10.1016/B978-0-08-042066-0.500215.

Haimson, B.C. & Cornet, F.H. (2003): ISRM suggested methods for rock stress estimation – Part 3: Hydraulic Fracturing (HF) and/or Hydraulic Testing of Pre-Existing Fractures (HTPF). International Journal Rock Mechanics and Mining Sciences 40/7-8, 1011-1020. DOI: 10.1016/j.ijrmms.2003.08.002.

Isler, A., Pasquier, F. & Huber, M. (1984): Geologische Karte der zentralen Nordschweiz 1:100'000. Herausgegeben von der Nagra und der Schweiz. Geol. Komm.

Jordan, P. (2016): Reorganisation of the Triassic stratigraphic nomenclature of northern Switzerland: overview and the new Dinkelberg, Kaiseraugst and Zeglingen formations. Swiss Journal of Geosciences 109, 241-255.

Nagra (2014): SGT Etappe 2: Vorschlag weiter zu untersuchender geologischer Standortgebiete mit zugehörigen Standortarealen für die Oberflächenanlage. Geologische Grundlagen. Dossier II: Sedimentologische und tektonische Verhältnisse. Nagra Technischer Bericht NTB 14-02.

Pietsch, J. & Jordan, P. (2014): Digitales Höhenmodell Basis Quartär der Nordschweiz – Version 2013 (SGT E2) und ausgewählte Auswertungen. Nagra Arbeitsbericht NAB 14-02.

Plumb, R., Edwards, S., Pidcock, G., Lee, D. & Stacey, B. (2000): The Mechanical Earth Model concept and its application to high-risk well construction projects. SPE Paper #59128 presented at the IADC/SPE Drilling Conference, New Orleans, Louisiana, February 2000. DOI: https://doi.org/10.2118/59128-MS.

Wileveau, Y., Cornet, F.H., Desroches, J. & Blumling, P. (2007): Complete in situ stress determination in an argillite sedimentary formation. Physics and Chemistry of the Earth Parts A/B/C 32/8-14, 866-878. DOI: 10.1016/j.pce.2006.03.018.